mater.scichina.com link.springer.com

Published online 3 June 2020 | https://doi.org/10.1007/s40843-020-1300-2
Sci China Mater 2020, 63(8): 1438–1463

SPECIAL ISSUE: Optical Gain Materials towards Enhanced Light-Matter Interactions

Growth of metal halide perovskite materials

Shaoli Wang[1,2], Fan Yang[2,3], Jiangrui Zhu[2], Qinxuan Cao[2,4], Yangguang Zhong[2], Aocheng Wang[2,3], Wenna Du[2] and Xinfeng Liu[2,5*]

ABSTRACT **Perovskite materials, especially metal halide perovskites, exhibit excellent properties, such as large optical coefficients, high carrier mobilities, long carrier lifetimes, tunable resistivities, large X-ray attenuation coefficients, and simple processing techniques. In recent decades, perovskites have attracted significant attention in the photoelectric field due to their versatile utility in solar cells, light-emitting diodes, photodetectors, X/γ-ray detectors, and lasing. However, the wide applicability of perovskites highly depends on the quality of perovskite crystals and films. Thus far, several perovskite growth technologies and methods have emerged. Therefore, this review classified and summarized the main methods that have been employed to achieve perovskite growth in recent years, including the solution temperature-lowering (STL) method, inverse temperature crystallization (ITC), anti-solvent vapor-assisted crystallization (AVC), spin coating, and chemical vapor deposition (CVD). Through analysis and summary, it has been determined that the STL, ITC, and AVC methods are mainly used to grow high-quality perovskite single crystals. While the spin-coating method has a significant advantage in the preparation of perovskite films, the CVD method is propitious in the fabrication of a variety of morphologies of micro/nano perovskite materials. We hope that this review can be a comprehensive reference for scientific researchers to prepare perovskite-related materials.**

Keywords: growth methods, perovskite, solution growth, spin-coating, CVD

INTRODUCTION

Perovskites, named after the Russian mineralogist, Perovski LA, initially referred to a calcium titanium oxide mineral composed of calcium titanate ($CaTiO_3$) [1]. Such terminology has since been extended to the kind of compounds that have a similar crystal structure as that of $CaTiO_3$. In 1958, Møller [2–4] first reported that $CsPbX_3$ (X=Cl, Br, I) compounds comprise the perovskite structure. Twenty years later, Weber [5,6] reported organic-inorganic hybrid metal halide perovskites by replacing cesium with methyl ammonium (MA) cations. One of the most important goals in materials science is the synthesis of new compounds, as well as the exploration of applying all known compounds [4]. Since Miyasaka and his colleagues [7] first used metal halide perovskite as a visible photosensitizer of photoelectron chemical cells in 2009, the research on the preparation and application of perovskite materials has been on a daily increase. With the development of research, it has been found that metal halide perovskites have many excellent properties, such as large optical coefficients [8,9], high carrier mobilities [10–12], long carrier lifetimes and diffusion lengths [13–15], as well as tunable resistivities [16], large X-ray attenuation coefficients, high fluorescence yields [16], wavelength tunability [17], and a simple processing technique [18,19]. Owing to these excellent properties, metal halide perovskite materials have become promising candidates for solar cells [20–28], lasers [29–33], luminescent devices [34–43], photodetectors [44–56], X-ray and γ-ray detectors [57], and so on, as shown in Fig. 1.

While the application of perovskite materials, in addition to the device structure, is impactful [58–60], two important factors need to be addressed: (i) the improvement in the material quality [61–63]; (ii) the development of different growth techniques [64–77]. The growth

[1] Experiment Center of Forestry in North China, Chinese Academy of Forestry, Beijing 102300, China
[2] CAS Key Laboratory of Standardization and Measurement for Nanotechnology, CAS Center for Excellence in Nanoscience, National Center for Nanoscience and Technology, Beijing 100190, China
[3] Department of Chemistry, School of Science, Tianjin University, Tianjin 300072, China
[4] School of Materials Science and Engineering, Zhejiang University, Hangzhou 310027, China
[5] University of Chinese Academy of Sciences, Beijing 100049, China
* Corresponding author (email: liuxf@nanoctr.cn)

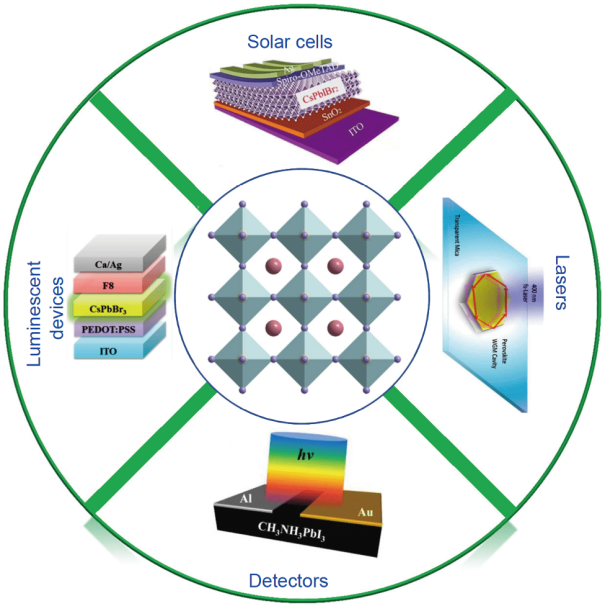

Figure 1 Main applications of metal halide perovskite materials. Reprinted with permission of the picture on the bottom from Ref. [50], Copyright 2016, the Royal Society of Chemistry; Reprinted with permission of the picture on the right from Ref. [31], Copyright 2014, the American Chemical Society; Reprinted with permission of the picture on the top from Ref. [28], Copyright 2019, the Royal Society of Chemistry; Reprinted with permission of the picture on the left from Ref. [35], Copyright 2015, the American Chemical Society.

processes have strong impacts on the material quality [78]. According to the different growth processes, the existing perovskite growth methods can be basically classified into the conventional solution growth method [64,68,79,80], and the "new solution method"—spin-coating [28,69,81,82] and chemical vapor deposition (CVD) [74,76,78,83–85]. The conventional solution growth approach mainly included the solution temperature-lowering (STL), inverse temperature crystallization (ITC), and the anti-solvent vapor-assisted crystallization (AVC) methods.

The conventional solution growth method is mainly used for the growth of perovskite single crystals, especially for the growth of bulk crystals. Owing to the fewer grain boundaries and the corresponding extremely low trap densities in the perovskite crystal, the perovskite crystals are more promising for realizing high-performance optoelectronic devices [17,86,87]. To prepare high-quality bulk perovskite single crystals, researchers have conducted several explorations and extensive research on the growth methods of perovskite single crystals. According to previous research, it has been discovered that the processes during the conventional solution growth methods of perovskite single crystals, such as the STL [1,79,88–90], ITC [91], and AVC methods [1,79,88–90], have significant influence on the quality of perovskite single crystals.

The "new solution method", i.e., the spin-coating, is one of the cheapest film production methods, which is widely used in solution-processed perovskite solar cells. Owing to the strong ionic interaction between metal ions and halogen anions, the evaporation and convective self-assembly processes in spinning immediately induced the formation of well-crystallized perovskite materials [91]. Although the spreading diffusion flow, which caused centrifugal force, was applied to the slowly evaporating solvent [91], the simple spin-coating could not produce a uniform perovskite layer on a large area [92]. Thus, a variety of methods have been explored to optimize the fabrication procedure, including one-step [28], two-step [93] and multi-step spin coating [71]. For the production of uniform perovskite films with large areas, the CVD method has been widely adopted in several studies, such as low vacuum single step processing [94], sequential deposition processing [95–100], hybrid CVD (HCVD) [78,99], and the hybrid physical-CVD (HPCVD) method [96], as well as growth under atmospheric conditions [101,102].

Herein, we classified and summarized the main methods that have been adopted for achieving perovskite growth in recent years, including the STL, ITC, AVC, spin coating, and CVD methods. Perovskites with different morphologies, such as bulk crystal, thin film, micro/nano platelet, nanowire, and micro/nano sphere, can be grown by different growth methods under different conditions. We hope, herein, that this review can provide a reference for scientific researchers in the selection of perovskite growth methods in the future.

GROWTH METHODS OF METAL HALIDE PEROVSKITES

The main growth methods of metal halide perovskites include the conventional solution, spin-coating, and CVD methods. Because of the versatility, simplicity, and low cost of the solution method, the conventional solution method occupies a prominent place in the growth of metal halide perovskites. Meanwhile, it is easier to grow high-quality single crystals, herein, compared with other methods. The spin-coating method is mainly used to fabricate perovskite thin films, which are mainly used to prepare solar cells. Furthermore, the spin-coating method is one of the least expensive film-forming methods. The CVD method is one of the numerous demonstrated ways

for the vapor deposition of perovskites. With the development of the CVD method, high-quality perovskite materials with different morphologies can be grown, such as platelets, films, micro-, and nanowires.

Solution method

STL growth method

The improved original Weber's method, which formed the solution temperature, has become one of the classical methods for the growth of metal halide perovskites. The driving force of the crystal growth is the solution supersaturation, which is achieved by gradually lowering the solution temperature. Therefore, the solute solubility of perovskite crystals grown by the STL method needs to decrease with the lowering of the solution temperature. In the first stage of STL method, the saturated solution is first prepared at a relatively high temperature, and then the solution is gradually cooled to a certain temperature in a certain time (approximately 24 h) for the precipitation of small seed crystals. In the second stage, the STL method can be divided into the bottom-seeded solution growth (BSSG) and the top-seeded solution growth (TSSG) methods, depending on the different fixed positions of the seed crystals, as shown in Fig. 2a, b. Summarily, the STL method initially synthesizes millimeter-sized crystals, and then, grows large-sized bulk single crystals by seed crystals.

Here, we introduce the research progress of the growth of metal halide perovskites by the BSSG method that has been adopted in recent years. In 1995, Mitzi and his coworkers [107] first prepared the cubic perovskite $CH_3NH_3SnI_3$ ($MASnI_3$) by precipitation from a hydriodic acid solution by the BSSG method. Initially, they gently heated the CH_3NH_2·HI and SnI_2 solutions in a water/ethylene glycol bath to 90°C and then mixed the solutions together. After mixing the warm solutions, the resulting yellow solution was cooled to room temperature. Finally, the black-green precipitate formed, which was then filtered under flowing N_2 and dried under flowing Ar at 100°C for 5 h. In 2014, Tao's group [64] obtained large-sized $MAPbI_3$ bulk single crystals by the BSSG method. The seeded crystal was fixed to the middle of a designed tray in the growth chamber. The tray fixing the seed crystal was rotated by an electric motor. Then, the saturated solution was slowly cooled from 65 to 40°C. After approximately one month, the single crystal $MAPbI_3$ with the dimension of 10 mm×10 mm×8 mm was successfully obtained in the bottom of the flask, as shown in Fig. 2e. It should be noted that in the STL method, the temperature of the precursor solution needs to maintain uniformity during the crystal growth process. To realize the temperature uniformity of the precursor solution in the growth process, the temperature of the solution can be controlled by utilizing a programmable temperature controller. In 2015, by decreasing the temperature of the growth solution from 100 to 57°C, Yan's group [108] also harvested centimeter-sized $MAPbI_3$ bulk single crystals *via* the BSSG method over the course of 15 d. In the process of seed growth, they found that $MAPbI_3$ could easily crystallize and some deposits appeared in the bottom of the flask, which coud easily adhere to the surface of the growing seed during the cooling process. The growth of large-bulk single crystal of $MAPbI_3$ was evidently hindered by the numerous formed crystal nuclei. To eliminate the negative effect, they fixed and supported the seed crystal with platinum wire to separate the seed crystal from the bottom of the flask. Later, Chen *et al.* [22] and Huang's team [109] noticed that the addition of chloride ions could control the morphological evolution and crystallinity of polycrystalline perovskite absorbers, thus improving the performance of the device. Therefore, by using chlorine as the medium of solution growth, they obtained large $MAPbI_3(Cl)$ single crystals of 20 mm×18 mm×6 mm in 5 d by the BSSG method. Regarding the chlorine promoters, not only was the growth rate evidently improved but also the crystal quality was higher, without compromising on the crystallinity, carrier mobility and carrier lifetime [65]. The growth cycle of the STL approach is effectively shortened from several weeks to several days by chlorine additive, which greatly reduced the cost of crystal preparation. Other kinds of perovskites, such as $MAPbBr_3$ [110], $MAPbCl_3$ [110], $MAPb(Cl_xI_{1-x})_3$ [111], $NH(CH_3)_3SnX_3$ (X=Cl, Br) [112], $FAPbI_3$ [113], and $FA_{(1-x)}MA_xPbI_3$ [114], have also been successfully prepared by the BSSG method.

To eliminate the influence of many seed crystals in the bottom of the flask during crystal growth *via* the BSSG method, many researchers chose to grow single crystals by the TSSG method. In 2015, Huang's group [103] reported large-sized $CH_3NH_3PbI_3$ ($MAPbI_3$) polycrystalline (MPC) growth from a supersaturated $MAPbI_3$ solution using the TSSG method with a temperature gradient, as shown in Fig. 2b. The $MAPbI_3$ single crystals (MSCs) gradually become larger by the consumption of small MSCs at the bottom. The small temperature difference between the bottom and the top of the solution created a small convection that is sufficient to transport the material to the large MSCs. Eventually, the obtained MSCs have an average size of 3.3 mm and a largest size of

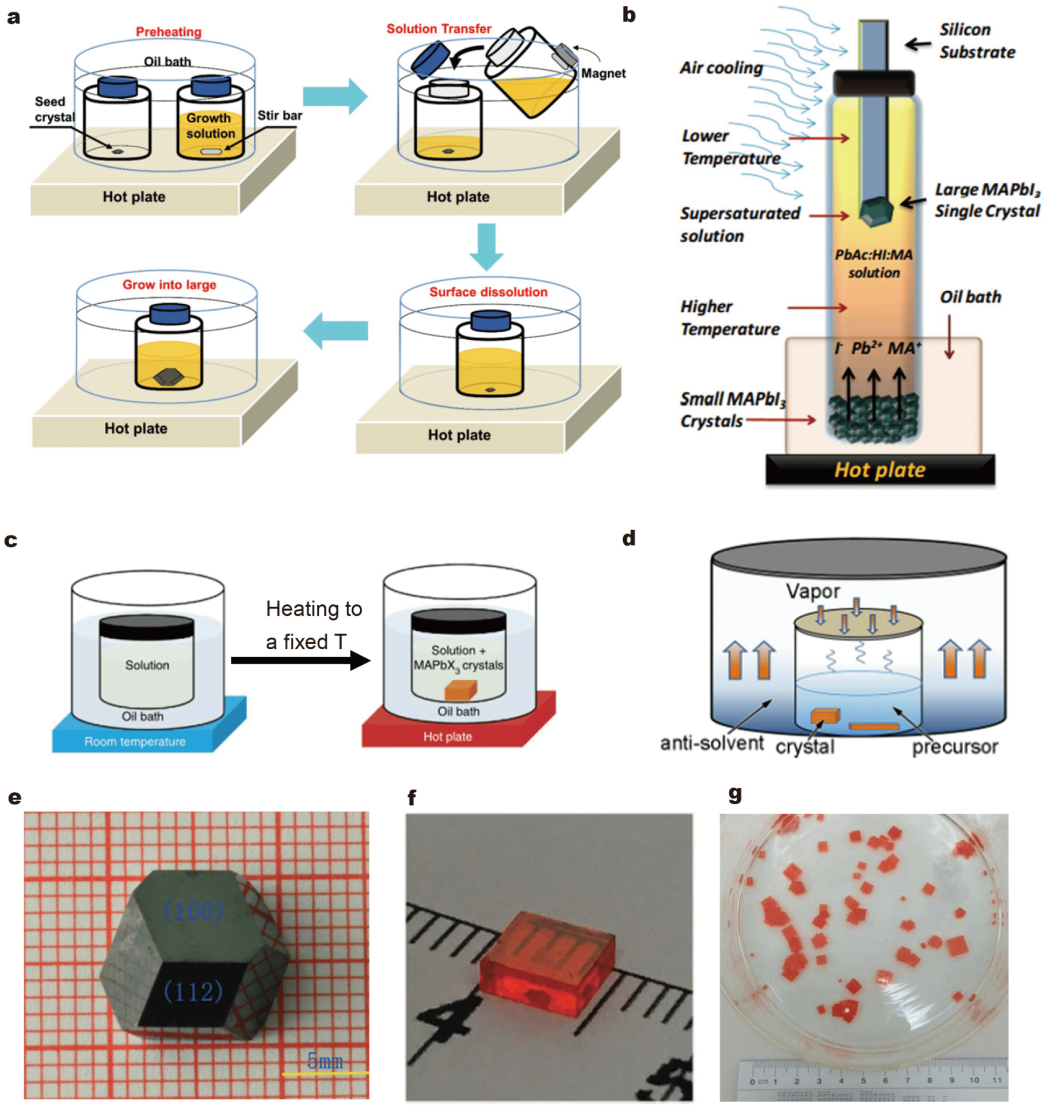

Figure 2 (a) Schematic of the BSSG method to grow large $MAPbI_3(Cl)$ bulk single crystals. Reprinted with permission from Ref. [65]. Copyright 2016, the American Chemical Society. (b) Schematic illustration of the TSSG method. Reprinted with permission from Ref. [103]. Copyright 2015, the American Association for the Advancement of Science. (c) Schematic representation of the ITC apparatus in which the crystallization vial is immersed within a heating bath. Reprinted with permission from Ref. [91]. Copyright 2015, the Springer Nature. (d) Schematic of the AVC method. Reprinted with permission from Ref. [104]. Copyright 2017, the American Chemical Society. (e) $CH_3NH_3PbI_3$ crystal by STL method. Reprinted with permission from Ref. [64]. Copyright 2014, the Royal Society of Chemistry. (f) $FAPbBr_3$ crystal grown by ITC method. Reprinted with permission from Ref. [105]. Copyright 2015, the Royal Society of Chemistry. (g) Crystallization of $MAPbBr_3$ by AVC method. Reprinted with permission from Ref. [106]. Copyright 2015, the American Association for the Advancement of Science.

~10 mm. The crystals are stable in air and could maintain the metal-like shinning surface for at least 6 months. In 2016, Tao's group [115] first obtained both cubic $CH_3NH_3SnI_3(MASnI_3)$ and $CH(NH_2)_2SnI_3$ ($FASnI_3$) single crystals under ambient atmosphere by the TSSG method, and the dimensions of single crystals reached 20 mm×16 mm×10 mm and 8 mm×6 mm×5 mm, respectively.

Summarily, STL methods provide a simple, convenient and applicable technique for the growth of bulk-sized perovskite single crystals. However, it is really time-consuming, and usually needs 2–4 weeks to harvest a single crystal of approximately 1 cm.

ITC growth method

Generally, the solubility of the precursor solution increases with an increase in temperature. However, there is

a relatively rare phenomenon that the solubility decreases with the temperature increase in some solutions. The inverse temperature-solubility behavior of $MAPbX_3$ perovskites in certain solvents was first found by Bakr's group [91]. According to this abnormal phenomenon, they developed the ITC method to grow $MAPbX_3$ single crystals (Fig. 2c), which is a rapid crystal growth approach. In the ITC method, crystals with controllable sizes and shapes can be formed in hot solution. Approximately 5-mm-length $MAPbI_3$ single crystals were obtained only in 3 h. The fastest growth rate of $MAPbBr_3$ single crystals was revealed to be up to 38 $mm^3\ h^{-1}$ at the third hour. The solvents and the growth temperatures were different under the condition of different halogens in the crystals. For example, the solvent of $PbBr_2$ and MABr in the precursor solution was *N*,*N*-dimethylformamide (DMF), while the solvent of PbI_2 and methylammonium iodide (MAI) was γ-butyrolactone (GBL). The bromide solution was usually prepared at room temperature (25°C), and the iodide solution needed to be heated to 60°C. The temperatures at which Br- and I-based crystals begin to grow also differ.

In practical applications, especially commercial applications, large-sized single crystals are needed. Liu's group [14] obtained inch-sized $MAPbX_3$ crystals with high crystallinity *via* the ITC method. They initially harvested the largest $CH_3NH_3PbI_3$ crystal that had dimensions of 71 mm×54 mm×39 mm, which exceeded half an inch. Liu's group not only grew a series of large single-halide perovskite crystals, including $CH_3NH_3PbCl_3$, $CH_3NH_3PbBr_3$, and $CH_3NH_3PbI_3$, but also grew large-scale dual-halide perovskite single crystals by the ITC method, which included $CH_3NH_3Pb(Cl_xBr_{1-x})_3$ and $CH_3NH_3Pb(Br_xI_{1-x})_3$, with the maximum crystal length reaching 120 mm [117].

The large-crystal growth process mainly included two steps: (i) the seed crystal was obtained in a supersaturated solution. When the precursor was heated to a certain high temperature and kept for 12 h, numerous small-sized seed crystals could be obtained from the supersaturated solution. (ii) High-quality seed crystals grew continuously in a fresh solution. By choosing one high-quality seed placed into the supersaturated precursor solution and kept for a certain period of time, the original seed grew to a larger crystal. To prepare larger crystals, the above-mentioned steps need to be continuously repeated [14,117].

In the ITC method, the key to growing a good single crystal is to choose the right solvent. After special investigation, Bakr's team [79,105] found that a specific solvent is most suitable for a specific halide perovskite. For example, they found that GBL is generally suitable for I-based perovskites, whereas the more polar DMF is the suitable solvent for the Br-based ones to induce retrograde solubility. Furthermore, they found that dimethylsulfoxide (DMSO) works best for $MAPbCl_3$. The retrograde behavior and ITC are not limited to the growth of $MAPbX_3$ perovskites, but can be extended to the growth of $FAPbX_3$ by solvent selection [79,105], as shown in Fig. 2f. When growing the $FAPbI_3$ crystal by the ITC method, the solvent used was GBL, and the temperature needed to be heated to 115°C. However, for the ITC method to grow $FAPbBr_3$, the solvent used was 1:1 (*v*/*v*) DMF:GBL, and the temperature at which the crystals began to grow was 55°C [79,113].

In addition to organic-inorganic hybrid halide perovskites, all inorganic halide perovskite single crystals can be grown by the ITC method. Using low-cost precursors, Kovalenko's team [116] prepared $CsPbBr_3$ single crystals in ambient atmosphere by the ITC method. They found that $CsPbBr_3$ was best grown in DMSO. Therefore, they dissolved CsBr:$PbBr_2$ in a mixture of DMSO with cyclohexanol (CyOH) and DMF to form the precursor solution, and heated it to 90°C in a vial, thereafter forming 1–3 nuclei. It was then heated to 110°C, resulting in further growth without additional nucleation. In a few hours, a flat, orange, and optically transparent single crystal with a length of approximately 8 mm was collected. Using MeCN and MeOH as solvents, Hodes's team [67] also obtained $CsPbBr_3$ single crystals by using a modified ITC method. To eliminate the appearance of undesirable precipitants (mostly the Cs_4PbBr_6), they used a two-step heating cycle. At first, they heated the solution to the required temperature for 4 h, and then decreased it to room temperature by continuous stirring. They found that there were no other retrograde soluble compounds except for the orange $CsPbBr_3$ crystal during the second heating cycle. The $CsPbBr_3$ crystal evidently appeared only above approximately 120°C in the MeCN-saturated solution, while the $CsPbBr_3$ crystal were apparent at approximately 40°C in the MeOH-saturated solution. It should be noted that only the bottom of the bottle can be heated to avoid crystal growth on the side of the bottle. Almost at the same time, Bakr's team [68] fabricated large and high-quality inorganic cesium lead halide single crystals using a similar ITC method. The production of CsBr and $PbBr_2$ is easy to form different compositions, including Cs_4PbBr_6, $CsPb_2Br_5$, and $CsPbBr_3$. They noted that the formation temperature of $CsPb_2Br_5$ was lower than that of $CsPbBr_3$. Therefore, CsBr and $PbBr_2$ were

dissolved in DMSO according to the molar ratio of 1:2 to form the precursor solution, which was filtered and heated to 120°C. Then, they harvested the isolated, millimeter-sized, rectangular, pure orange $CsPbBr_3$ crystals. Choosing DMF as the solvent, they obtained a needle-like, yellow phase of $CsPbI_3$ by a similar technique.

In the ITC method, the crystallization is induced by the solubility, which is inversely proportional to the temperature, in a specific organic solvent, and the whole crystal growth process is completed in a few hours. The ITC method is much faster than the STL method; therefore, the former is mainly used to rapidly grow larger-sized single crystals of metal halide perovskites.

AVC growth method

Based on the different solubilities of perovskite compounds in different solvents, the AVC crystal growth method was developed [1,79,88–90]. It was reported that $MAPbI_3$ films were prepared by thermal evaporation from the precursor with Cl^--based metal salt. Then, they found that the carrier diffusion lengths of the films were two times longer than those of the best solution-treated material [10,124]. To obtain high-quality perovskite films, Tidhar's team [125] introduced the concept of anti-solvent-assisted crystallization into the sample preparation for the first time in 2014. Inspired by those, Bakr's team [106] first obtained high-quality $MAPbX_3$ with millimeter-scale *via* the AVC method, as shown in Fig. 2g. Fig. 2d shows the scheme of the AVC method. They dissolved MAX and PbX_2 in DMF or *g*-butyrolactone (GBA) to prepare the precursor, and used dichloromethane (DCM) as an anti-solvent to prepare the $MAPbX_3$ crystal. In another report, Yang's group [118] selected DMF as the precursor solvent and toluene as the anti-solvent to induce crystallization of $MAPbBr_3$. At last, they obtained orange block-shaped single crystals by the AVC method. Using DMF/DCM as the solvent/anti-solvent, Loi's group [119] grew a few millimeter-sized $MAPbBr_3$ single crystals with a self-made simple device by the AVC method in several days. Similarly, Zhang's group [122] reported that $MAPbI_3$ single crystals were grown by an improved AVC method in diethyl ether (DE) as the anti-solvent. Using acetonitrile and iodate/DE as precursors/anti-solvent, Grancini's group [123] obtained dark, highly reflective block $MAPbI_3$ single crystals by the AVC method. Using DMF/DCM as the solvent/anti-solvent, Liao's group [120] initially synthesized single-crystalline, square micro disks (MDs) of $MAPbBr_3$ by a modified AVC method, which was named the "one-step solution self-assembly method". The four sides of the obtained $MAPbBr_3$ constitute a built-in whispering-gallery mode microresonator, and the quality factor reached a value of approximately 430. To understand the growth mechanism of $MAPbBr_3$ crystals, Xu's group [121] synthesized the intermediate states of these crystals on filter paper by using the modified AVC method, which is similar with the "one-step solution self-assembly method" of Liao's group. Bakr's team [126] was concerned that macro-perovskite crystals could not grow on flat substrates, limiting their potential for optoelectronic integration. Thus, they synthesized large-area $MAPbBr_3$ crystalline films using the AVC crystallization technique, which entailed large perovskite single crystals. The mobility and diffusion length of crystal films are similar to those of single crystals. The key operation involved was introducing a stirring force into the crystallization dish in the modified AVC method, which could be used to prepare two-dimensional integrated single-crystal perovskites.

Inorganic perovskite crystals can also be grown by the AVC method. Rakita's team [67] obtained $CsPbBr_3$ single crystals by a modified AVC method. In this method, the precursor solution was formed by the CsBr and $PbBr_2$ dissolved in DMSO at 50°C and MeCN or MeOH was selected as the anti-solvent. The key step of this method was to add a pre-saturation step, which could prevent undesired Cs_4PbBr_6 from settling along the side of the required $CsPbBr_3$. After optimization, $CsPbBr_3$ perovskite crystals with a millimeter scale and 100% yield can be grown without seed crystal. There are three different phases of cesium lead bromine, including $CsPbBr_3$, $CsPb_2Br_5$, and Cs_4PbBr_6. Therefore, obtaining high-quality large-sized $CsPbBr_3$ crystals by the AVC method remains a challenge. Zhang's group [104] has grown $CsPbBr_3$ crystals from a low temperature solution by the AVC method, where the largest $CsPbBr_3$ crystals reached 42 mm×5 mm×3 mm. After analyzing the phase diagram of cesium lead bromine, they got the optimized AVC method, in which the ratio of $PbBr_2$ and CsBr was 1.5 in the precursor, while 50% MeOH and 50% DMSO were selected as the anti-solvent. Under optimized conditions, Ding's team obtained orthorhombic $CsPbBr_3$ single crystals using DMSO/MeOH as solvent/anti-solvent by the AVC method. The growth temperature and the diffusion rate of anti-solvent methyl alcohol can affect the growth process of $CsPbBr_3$ single crystals. By adjusting the temperature to 40°C and controlling the diffusion rate of methyl alcohol vapor in the growth solution (adjusting the number of pores), $CsPbBr_3$ single crystals with different shapes were successfully grown [127]. The anti-

solvent plays an important role during the growth of inorganic perovskite single crystals by the AVC method. If DMSO/DE is selected as a solvent and anti-solvent pair, Cs_4PbBr_6 crystallites can be obtained under similar conditions. Therefore, the researchers believed that the final crystallization products in the AVC method were determined by the miscibility of the solvent and the anti-solvent. Thus, it is demonstrated that the high miscibility (such as MeOH in DMSO) initially produces $CsPbBr_3$ and then $CsPb_2Br_5$; while low miscibility (such as DE in DMSO) directly produces Cs_4PbBr_6 [128].

Using the AVC method, perovskite thin film crystals or nanowire arrays can also be grown. Bakr's group [129] successfully prepared and characterized the hybrid perovskite monocrystalline films on substrates by using a modified AVC method that they termed cavitation-triggered asymmetrical crystallization (CTAC). This method overcomes the shortcomings of traditional single-crystal growth methods in its tendency to produce merely free-standing perovskite single crystals.

The CTAC strategy would promote heterogeneous nucleation by providing enough energy to overcome the nucleation barrier. Briefly, to obtain the perovskite films, a very short ultrasonic pulse (≈1 s) was introduced into the solution when the solution reached a low supersaturation with anti-solvent vapor diffusion, which is the key contribution of the CTAC method [129]. Pan's group [130] achieved the fabrication of large-area inorganic perovskite monocrystalline thin films by a space-limited AVC method. The schematic illustration of the inorganic perovskite monocrystalline thin films growth is shown in Fig. 3a. A stock solution (50 μL) of equimolar CsBr and $PbBr_2$ in DMSO was spread on a 2.5 cm×2.5 cm hydrophilic substrate. Then, another octadecyltrichlorosilane (OTS)-treated hydrophobic substrate was brought into contact with the DMSO solution, and the two clean flat substrates were clipped together. Pressure was applied uniformly on the two substrates. The bubbles in the solution were eliminated by a few seconds of vacuum pumping. Then, they were placed in a sealed glass beaker, which contained acetonitrile (CH_3CN). The glass beaker can be put in a 40°C oven to boost the growth rate. Since CH_3CN is a poor solvent for $CsPbBr_3$ and its dielectric constant is close to that of DMSO, a slow diffusion of CH_3CN vapor into DMSO solution would induce the nucleation of $CsPbBr_3$ (Fig. 3a-iii) rather than CsBr-rich Cs_4PbBr_6 or $PbBr_2$-rich $CsPb_2Br_5$, and the subsequent growth of $CsPbBr_3$ monocrystalline films between two clipped substrates [130].

$CsPbBr_3$ has excellent optoelectronic properties and shows great potential in laser applications. In particular, $CsPbBr_3$ nanowire arrays with controlled growth size and position are conducive to cost-effective and large-scale expansion to on-chip devices. Pan's group [131] successfully obtained a $CsPbBr_3$ microwire (MW) single crystal array with adjustable width, length, and position by using a polydimethylsiloxane (PDMS) template-confined AVC method. Briefly, the equimolar CsBr and $PbBr_2$ were dissolved in DMSO at 50°C. After titration with MeCN until the orange precipitate disappeared, the precursor solution was formed. The PDMS template was brought into contact with the DMSO solution and the pressure was applied uniformly on the PDMS to drive the solution into the void space of the PDMS template. Then, the SiO_2/Si substrates coated with the precursor solution were put into a crystallizing dish containing CH_3CN. The $CsPbBr_3$ MWs can crystallize with the diffusion of CH_3CN vapor into the precursor solution. With the extension of reaction time, the DMSO in the precursor solution gradually volatilized and the MWs gradually became

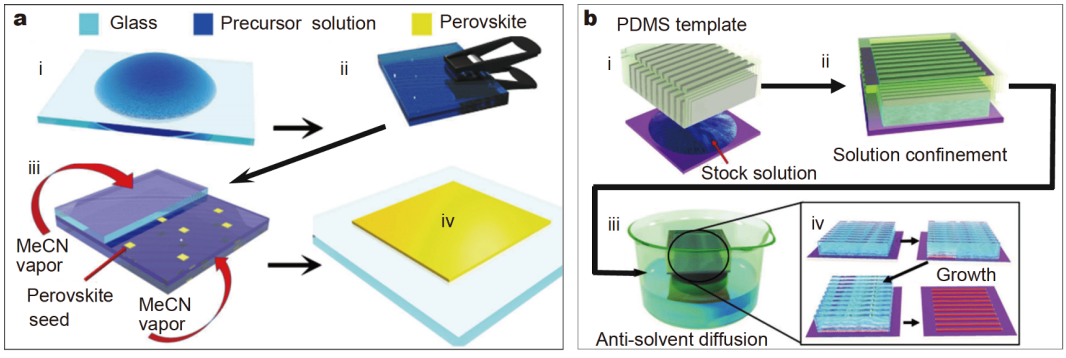

Figure 3 (a) Schematic diagram for growth of $CsPbBr_3$ monocrystalline films. Reprinted with permission from Ref. [130]. Copyright 2018, Wiley. (b) Schematic diagram showing the entire preparation procedure of $CsPbBr_3$ MW arrays using the PDMS template-confined anti-solvent crystallization method. Reprinted with permission from Ref. [131]. Copyright 2019, Wiley.

longer. After 12 h, the entire reaction system was collected, washed with CH_3CN, thermally dried, and refilled with a new precursor solution (without peeling off the PDMS). After repeating the above-mentioned steps, the PDMS templates can be peeled off from the substrates. Finally, the MW arrays can be obtained after washing with CH_3CN and drying with N_2 stream. This method is relatively easy to prepare large-scale $CsPbBr_3$ MW arrays with controlled width, length, and position.

In the AVC method, DMF, DMSO, and GBL are commonly used as good solvents during the growth of metal halides, while chlorobenzene, chloroform, benzene, xylene, 2-propanol, toluene, DE, and acetonitrile are often used as anti-solvents. However, choosing the right solvent/anti-solvents is key to crystal growth. Therefore, it is essential to choose the appropriate solvent/anti-solvent, according to the specific reaction system. The AVC method has a relatively low dependence on temperature during crystal growth. Compared with the STL and ITC methods, it is generally difficult to obtain large-sized single crystals by the AVC method.

In the STL method, the crystal growth rate is slow because of the small daily temperature drop and the small supersaturation. However, due to the large volume of the solution and the long growth time, it is easy to grow large-scale and high-quality perovskite single crystals. In the ITC method, because the solution temperature rises to a certain level in a relatively short period of time, the supersaturation of the solution is large. Therefore, the ITC method can generally form perovskite single crystals with medium sizes in a relatively short period of time, as shown in Table 1. In the AVC method, with the diffusion of the anti-solvent in the solvent over a period of time, the solution will reach the critical value of supersaturation in an instant, and a large number of crystal nuclei will form and grow gradually. Therefore, perovskite single crystals grown by the AVC method are usually small in size and large in number.

Spin-coating method

The spin-coating method is also adopted in preparing perovskite materials. This method is a low-cost film production method and mainly used in solar cells of solution-processed perovskites. Summarily, the growth of perovskite crystals in spin-coating involves three processes: the solution reaches supersaturation, nucleation, and subsequent growth towards a large crystal [132–136]. Firstly, the solvent rapidly evaporates when the precursor solution is dropped on the substrate, then the concentration of the solute increases, and the precursor solution can quickly reach saturation (C_s). At this point, however, nucleation cannot occur owing to the critical energy barrier. As the solvent continues to evaporate, when the solution reaches supersaturation (C_{ss}) and the Gibbs free energy is above the energy barrier, the new crystal nuclei can form. Secondly, more crystal nuclei are formed and gradually grow with the continuous evaporation of the solvent. With the steady formation of crystal nuclei and the gradual growth of crystals, an increasing amount of solutes will be consumed. When the solution concentration is lower than C_{ss}, the nucleation process can stop, while for the solution concentration lower than the C_s, the new formed crystal can stop growing. Generally, GBL, DMSO, DMF and *N*-methyl-2-pyrrolidone are selected as the solvents for lead halide and MAI. However, although the convection diffusion due to the centrifugal force during the spin-coating process facilitates the slow evaporation of the solvent, simple spin-coating cannot produce a uniformly thick perovskite layer over a large area [92]. The quality of perovskite films plays a key role in the photovoltaic performance of perovskites. Tight and well-crystallized perovskite films are a prerequisite for the preparation of high-efficiency solar cells [137].

N-step methods spin-coating

(1) One-step method

Due to the volatility and hygroscopic properties of organic cations, such as $CH_3NH_3^+$ (MA^+) and $CH_3(NH_2)^{2+}$ (FA^+) [93,129,138], hybrid perovskites have some instabilities, which become huge obstacles to their development. Therefore, the inorganic perovskite with Cs^+ and Rb^+ cations has attracted great interest in development. Yin's team [28] obtained a high-quality $CsPbIBr_2$ film through a simple one-step spin-coating method with a preheating process. The process of preparing the $CsPbIBr_2$ perovskite thin film by the preheating-assisted spin-coating approach, is shown in Fig. 4a. Initially, the SnO_2/ITO substrates were placed on a hot plate for 10 min. Then at room temperature, the $PbBr_2$ and CsI were dissolved in DMSO to prepare the $CsPbIBr_2$ precursor. The precursor solution was spin-coated on a preheated SnO_2/ITO substrate at 5000 r min^{-1} for 60 s, and then, the perovskite film was obtained after a two-step annealing process. After the substrate was preheated, the residual heat on the substrate could accelerate the evaporation rate of the solvent, which played a key role in improving the quality of the film. After optimization, high coverage and high crystallinity helped to generate more light-induced carriers in $CsPbIBr_2$ films and re-

Table 1 Typical metal halide perovskite crystals grown by solution methods

Growth method	Crystal	Ratio of raw material	Solvent/ anti-solvent	Growth temperature T (°C)	Growth time	Crystal color	Crystal size	Ref.
BSSG	$MASnI_3$	CH_3NH_2·HI/ SnI_2=1:1	HI	90–RT[a]	–	Black-green	–	[107]
	$NH(CH_3)_3$ $SnCl_3$	$SnCl_2$·$2H_2O$/ $NH(CH_3)_3Cl$=1:1	$HCl+H_3PO_2$	54–RT	One month	Colorless	13 mm×8 mm ×6mm	[112]
	$NH(CH_3)_3$ $SnBr_3$	SnO/$NH(CH_3)_3$ Cl=1:1	$HBr+H_3PO_2$	56–RT	One month	Colorless	8 mm×6 mm× 4 mm	
TSSG	$MAPbI_3$	$Pb(Ac)_2$·$3(H_2O)$/ MAI=1:1	Aqueous HI	65–40	One Month	Black	10 mm×10 mm× 10 mm	[64]
	$MAPbI_3$	$Pb(Ac)_2$·$3(H_2O)$, CH_3NH_2	HI	100–57	15 d	Black	12 mm×12 mm× 7 mm	[108]
	$MAPbI_3$	$Pb(Ac)_2$·$3(H_2O)$/ CH_3NH_2=1:2	HI	75	Several days	Black	largest size of ~10 mm	[103]
	$MASnI_3$	SnO/MAI=1:1	HI/H_3PO_2=1:1	65	One month	Black	20 mm×16 mm× 10 mm	[115]
	$FASnI_3$	SnO/FAAc=1:1	HI/H_3PO_2=1:1	60	One month	Black	8 mm×6 mm× 5 mm	
ITC	$CsPbBr_3$	$CsBr/PbBr_2$=1:2	DMSO+DMF	100–120	3 h	Orange	3 mm×2 mm ×1 mm	[68]
	$CsPbBr_3$	$CsBr/PbBr_2$=1:1	MeOH	RT–80	6 h	Orange	Nearly 3 mm long	[67]
	$CsPbBr_3$	$CsBr/PbBr_2$=1:2	DMSO+CyOH +DMF	90–110	Several hours	Orange	Nearly 8 mm long	[116]
	$FAPbBr_3$	$FAPbBr_3$	DMF/GBL=1:1	40–60	5 h	Orange	Nearly 5 mm long	[105]
	$FAPbI_3$	$FAPbI_3$	GBL	20–115	3 h	Black	3 mm long	[105]
	$MAPbI_3$	PbI_2/MAI=1:1	GBL	50–100	2 d	Black	120 mm×70 mm ×52 mm and 113 mm ×58 mm ×52 mm	[117]
AVC	$CsPbBr_3$	$CsBr/PbBr_2$=1:1	DMSO/MeCN	50	48 h	orange	Nearly 5 mm long	[67]
	$CsPbBr_3$	CsBr/ $PbBr_2$=1.5:1	DMSO/50% DMSO+50% MeOH	RT	3–14 d	Orange	42 mm ×5 mm× 3 mm	[104]
	$MAPbBr_3$	$PbBr_2$/MABr=1:1	DMF/ Toluene	RT	>3 d	Orange	1.4 mm×1.4 mm× 0.7 mm	[118]
	$MAPbBr_3$	$PbBr_2$/MABr=1:1	DMF/DCM	RT	Several days	Orange	A few millimeters	[119]
	$MAPbBr_3$	$PbBr_2$/MABr=1:1	DMF/DMC	25	24 h	Orange	10 μm×10 μm ×300 nm	[120]
	$MAPbBr_3$	$PbBr_2$/MABr=1:1	DMF/DMC	60	Different time	Orange	–	[121]
	$MAPbI_3$	PbI_2/MAI=1:1	HI/DE[b]	RT	2 d	Black	Nearly 1 mm long	[122]
	$MAPbI_3$	PbI_2/MAI=1:1	C_2H_3N+HI/DE	RT	2 d	Black	–	[123]

a) RT, room temperature; b) DE, diethyl ether.

duced recombination. This method provided an effective way to prepare high-quality inorganic perovskites [28]. Yang's team [139] obtained the $MAPbI_3$ perovskite by a one-step method. It is significant that a gas pump drying system was introduced to accelerate solvent evaporation in the preparation of $MAPbI_3$ film. Li's team [140] obtained shiny and smooth $FA_{0.81}MA_{0.15}PbI_{2.51}Br_{0.45}$ crystalline perovskite films by introducing a simple vacuum-flash solution processing to the one-step method.

(2) Two-step method

Different from the traditional organic-inorganic hybrid perovskites, a convenient two-step method invented by Jin's team [138] to prepare inorganic perovskites, including $CsPbBr_3$, $CsPbIBr_2$, and $CsPb_{0.9}Sn_{0.1}IBr_2$, can be carried out without humidity control. The approximate preparation process is as follows: firstly, the solid pre-

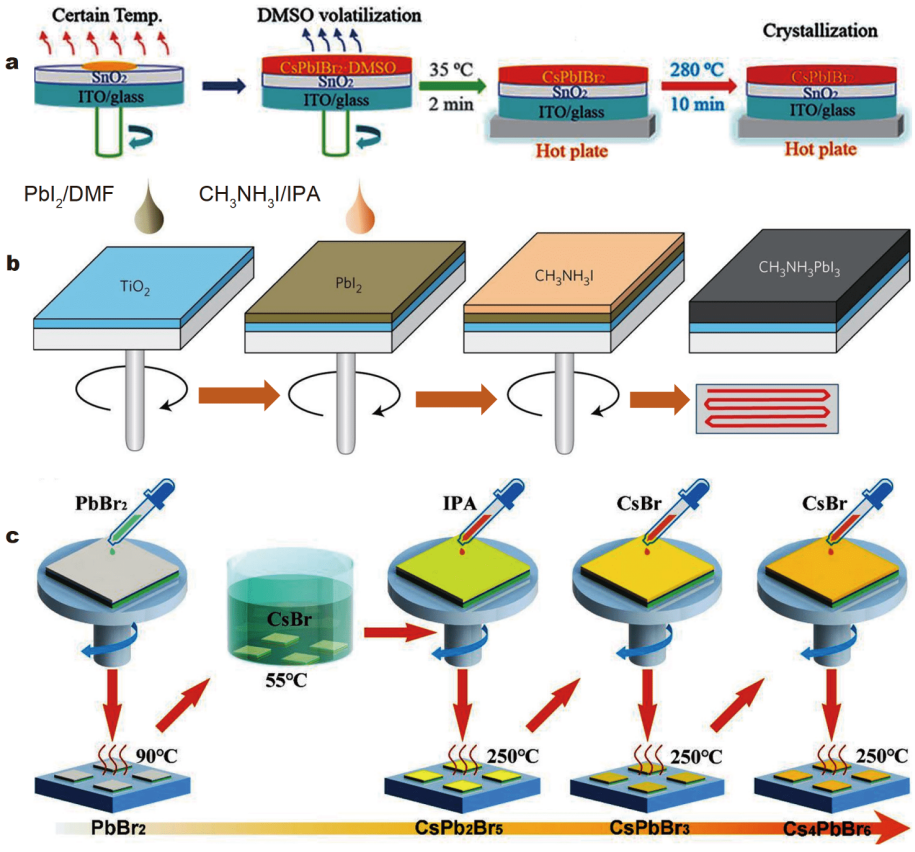

Figure 4 (a) One-step spin-coating method. Reprinted with permission from Ref. [28]. Copyright 2019, the Royal Society of Chemistry. (b) Two-step spin-coating method. Reprinted with permission from Ref. [93]. Copyright 2014, Springer Nature. (c) Multi-step spin-coating method. Reprinted with permission from Ref. [71]. Copyright 2019, Elsevier.

cursor ($PbBr_2$ for $CsPbBr_3$ and $CsPbIBr_2$; or the mixture of $PbBr_2$ and $SnBr_2$ with a molar ratio of 0.9:0.1 for $CsPb_{0.9}Sn_{0.1}IBr_2$) was dissolved in the mixed solvents of DMF and DMSO (4:1, *v*/*v*) under stirring at 80°C for 30 min to yield a 1.0 mol L^{-1} precursor solution. Then, the solution was deposited on the fluorine doped tin oxide (FTO)/c-TiO_2/m-TiO_2 substrate by spin-coating at 2000 r min^{-1} for 30 s, and dried at 80°C for 30 min. After that, the prepared film was dipped in a 15 mg mL^{-1} methanol solution of cesium salt (CsBr for $CsPbBr_3$; or CsI for $CsPbIBr_2$ and $CsPb_{0.9}Sn_{0.1}IBr_2$) for 10 min. Subsequently, the as-obtained yellow films were thoroughly rinsed with isopropanol, and then heated for 10 min in air on a hotplate (250°C for $CsPbBr_3$; or 350°C for $CsPbIBr_2$ and $CsPb_{0.9}Sn_{0.1}IBr_2$). Then, $CsPb_{0.9}Sn_{0.1}I_2Br$ and $Cs_{0.9}MA_{0.1}Pb_{0.9}Sn_{0.1}IBr_2$ films were also prepared by a similar process.

The growth of $CH_3NH_3PbI_3$ cuboids can be realized with a controlled size by a two-step spin-coating method invented by Park's team. The average efficiency of the solar cell made from this $CH_3NH_3PbI_3$ perovskite exceeded 16% and the best efficiency could reach 17%. The two-step spin-coating procedure was described schematically in Fig. 4b [93].

Summarily, a 1 mol L^{-1} solution of PbI_2 in DMF was initially spin-coated onto a TiO_2 blocking layer with a mesoporous TiO_2 film deposited. The PbI_2-coated film was dried at 40°C for 3 min and 100°C for 5 min. In the second step, different concentrations of CH_3NH_3I in 2-propanol solution were spin-coated onto the PbI_2 film and dried at 100°C for 5 min to form $MAPbI_3$ [63]. They found that the size of the cuboid $CH_3NH_3PbI_3$ was related to the concentration of CH_3NH_3I and its cuboid size significantly affected the charge-carrier extraction and light-harvesting efficiency [93]. Using a similar two-step spin-coating technique, Meng's team [141] first spin-coated the mixed solution of CH_3NH_3Cl and CH_3NH_3I onto a TiO_2/PbI_2 film to form a controllable morphology of $CH_3NH_3PbI_{3-x}Cl_x$ film. They speculated that the existence of CH_3NH_3Cl would lead to preferential growth

along the [110] direction of the perovskite, which could increase the crystallinity and surface coverage of the perovskite and reduce pinholes. Sang Il Seok's team [142] introduced additional iodide ions into the organic cation solution by the two-step method, which were used to form the perovskite layers through an intramolecular exchanging process, decreasing the concentration of the deep-level defect.

(3) Multi-step method

Owing to its excellent stability, especially thermal stability, the all-inorganic $CsPbBr_3$ perovskite solar cell has attracted great attention in the photovoltaic field in recent years. However, bromide-rich perovskites, such as $CsPbBr_3$, are always plagued by the low-phase purity and poor morphology of traditional two-step deposition methods [17,18]. Liao's team [71] demonstrated a simple and improved multi-step spin-coating process for manufacturing high-quality $CsPbBr_3$ films, as shown in Fig. 4c. The process of multi-step spin-coating method was as follows: firstly, the $PbBr_2$ in DMF solution was spin-coated onto a substrate and annealed at 90°C. Secondly, the $PbBr_2$ film was immersed in a CsBr methanol solution maintained at 55°C. Then, the formed $CsPbBr_3$ film was washed with isopropyl alcohol, and annealed at 250°C to crystallize. Eventually, the surface of the $CsPbBr_3$ film needed to be further spin-coated with CsBr methanol solution. Compared with the film prepared by the traditional two-step deposition process, the films prepared by the multi-step spin-coating method had higher homogeneity, higher $CsPbBr_3$ phase purity, and larger average grain size (up to 1 μm). More importantly, not only the power conversion efficiency (PCE) of the $CsPbBr_3$ perovskite solar cells was significantly boosted, but also the unencapsulated $CsPbBr_3$ perovskite solar cell presented good humidity and thermal stability when stored in ambient air at room temperature (25°C) for over 1000 h and at 60°C for one month, respectively. The multi-step spin-coating method provides a way for the practical application of efficient, cost-effective, and stable all-inorganic perovskite solar cells.

Doping method

The bromide compound, $MAPbBr_3$, has a band gap of approximately 2.3 eV, and it is chosen as one of the candidates for visible laser and luminescence applications [143,144]. Photoluminescence quantum yield (PLQY) is an important indicator for both applications. A new doping method was invented by Sessolo's team [145] to produce the high-PLQY perovskite-based materials, whereby the stable alumina nanoparticles (NPs) were blended to the perovskite precursor. The $PbBr_2$ and MABr were mixed together in a certain ratio and dissolved in DMF to form the precursor solution. Subsequently, an aqueous dispersion of Al_2O_3 NPs with an average size of 10 nm was added to the perovskite precursor. The composite thin films can be prepared by spin-coating the mixture solution on substrate in air, and then annealed on a hot plate at 90°C for 1 h. The size of the nanocrystals depended on the concentration and size of the Al_2O_3 NPs. They found that the self-assembly of Al_2O_3 NPs limited the growth of perovskite to nanoscale, which resulted in the spontaneous formation of isotropic $MAPbBr_3$ nanocrystals. Therefore, a strong enhancement of photoluminescence can be observed. In addition, the material was simple to handle from the solution and insensitive to moisture, which made it become an interesting candidate for laser applications and luminescence.

Inorganic cesium lead perovskite ($CsPbI_3$) is a promising material that can prepare wide band gap perovskite solar cells, but it is unstable at room temperature. Therefore, the stabilization of the α-phase of $CsPbI_3$ was one of the key prerequisites for its photovoltaic applications. A simple method to stabilize α-phase $CsPbI_3$ film by a single-step spin-coating process was reported by Huang's team [72], as shown in Fig. 5b, c. An equal molar ratio of PbI_2 and CsI dissolved in the mixed solvent DMSO/DMF (1:4, *v*/*v*) to form the $CsPbI_3$ precursor [72]. The $CsPbI_3$ precursor solution was added to three different sulfobetaine zwitterions to stabilize the α-phase $CsPbI_3$ film, as shown in Fig. 5b. They found that the best ratio of zwitterion added into $CsPbI_3$ solution was 1.5%, in which the α-phase $CsPbI_3$ film can be stabilized at room temperature. The interaction between zwitterions and $CsPbI_3$ hindered the rapid crystallization of $CsPbI_3$, such that the grain size of $CsPbI_3$ and the stabilization of the α-phase could be reduced, as shown in Fig. 5c. It was found that zwitterions prevented the crystallization of $CsPbI_3$ perovskite films by electrostatic interaction with ions and colloids in the $CsPbI_3$ precursor solution. The PCE of the solar cell using zwitterion-stabilized perovskite thin film can be attained at 11.4% under 1-sun illumination [72].

The long-chain ammonium salt additives were selected as the surface capping ligands during the one-step thin film spin coating by Jin's group [81], which could stabilize the metastable state during the film deposition of the $CsPbI_3$ perovskite structure. It was found that different ammonium ligands can selectively stabilize two different perovskite polymorphs, including the cubic α-$CsPbI_3$ and the orthorhombic β-$CsPbI_3$ phase with distorted per-

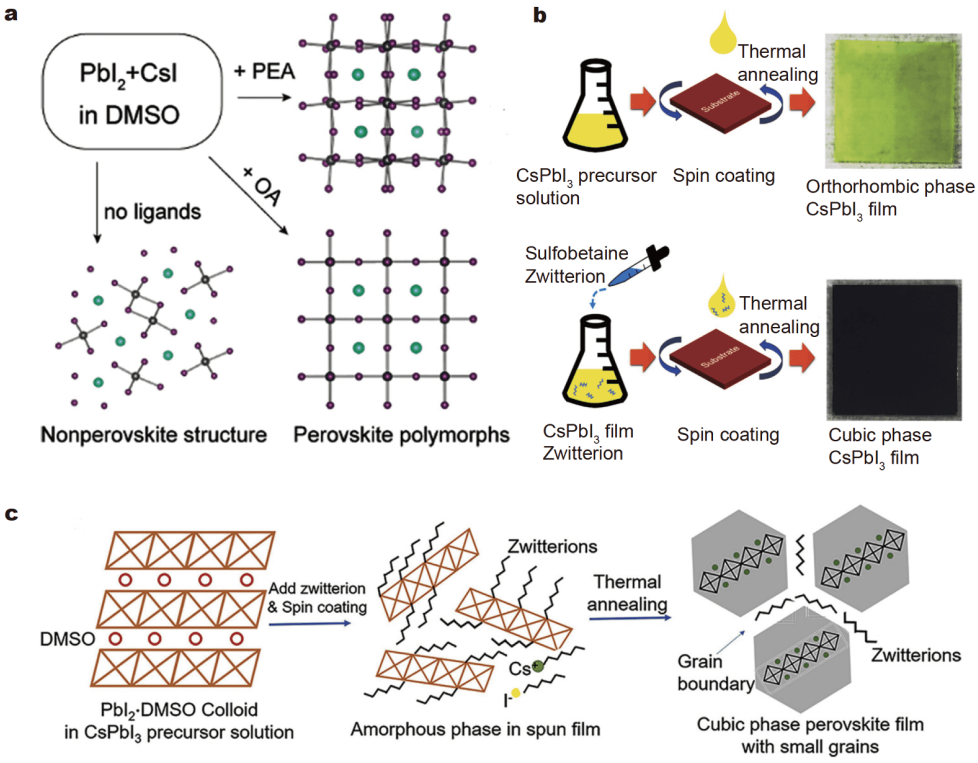

Figure 5 (a) Schematic illustration of hypothesized surface ligand functionalization of the $CsPbI_3$ perovskite structures and structural characterizations of the stabilized $CsPbI_3$ thin films. Reprinted with permission from Ref. [81]. Copyright 2017, the American Chemical Society. (b) The fabrication scheme of $CsPbI_3$ film without/with zwitterions by one-step spin-coating. Reprinted with permission from Ref. [72]. Copyright 2017, Elsevier. (c) Schematic representation of $CsPbI_3$ crystal formation from precursor solution with zwitterion. Reprinted with permission from Ref. [72]. Copyright 2017, Elsevier.

ovskite structure, as shown in Fig. 5a. Through surface functionalization, the $CsPbI_3$ perovskite film had excellent room-temperature phase stability and exhibited good photophysical properties. It can be indicated that the spin-coating can provide a new way to obtain the optoelectronic devices based on $CsPbI_3$ perovskites [81].

To get a film with more uniform and tightly distributed grains, ZnO NPs were introduced into the $CsPbBr_3$ precursor solution [70]. The $CsPbBr_3$ and $CsPbBr_3$:ZnO precursor needed to be prepared in an N_2 glovebox. The CsBr and $PbBr_2$ dissolved in the DMSO solvent to form the $CsPbBr_3$ precursor solution. Adding ZnO NPs to the $CsPbBr_3$ precursor solution at 60°C for 30 min can result in the formation of the $CsPbBr_3$:ZnO precursor solution. The spin-coating process can improve the morphology and surface coverage of the film [69,146–148]. Therefore, the preparation of the $CsPbBr_3$ and $CsPbBr_3$:ZnO thin films introduced the spin-coating process. Through spin coating, the precursor solutions of the $CsPbBr_3$ or $CsPbBr_3$:ZnO, the perovskite $CsPbBr_3$ and $CsPbBr_3$:ZnO films can be obtained. To wash away the DMSO from the perovskite wet film, 1 mL of chlorobenzene needs to be pipetted onto the substrate (15 s) before the last spin-coating step [69,147,148]. To remove the residual DMSO solvent, an annealing process was also needed. The performance of photodetectors made with all-inorganic $CsPbBr_3$:ZnO was better than that without ZnO doping [68].

Owing to its environmental stability, proper band gap, and distinctive color, $CsPbIBr_2$ has broad photovoltaic application prospects. However, the defect states on the grain boundaries and the surface of the $CsPbIBr_2$ polycrystalline film can cause non-radiative carrier recombination, which reduces the final PCEs of its corresponding perovskite solar cells. Zheng's group [137] passivated the defect states of pure $CsPbIBr_2$ film by adding polyethylene glycol (PEG) into the precursor solution of $CsPbIBr_2$ to improve the film morphology and coverage. Firstly, the precursor solution of $CsPbIBr_2$ doped with a small amount of PEG was spin-coated on the corresponding substrate, and then, subsequently annealed to form a PEG-passivated $CsPbIBr_2$ film. After

introducing the PEG, not only the wettability of the precursor solution can be improved but also the coverage of the perovskite film on substrate can be enhanced owing to the three-dimensional (3D) network framework of PEG. In addition, the growth rate of the crystals can be slowed down and the aggregation of the perovskite crystals can be inhibited by the self-assembled PEG network in the process of the formation of the perovskite phase. In this way, it can effectively passivate the defect states at the surface and grain boundaries of $CsPbIBr_2$ film, which can result in a more uniform perovskite film with fewer voids [137].

Other methods of spin-coating

(1) Intermolecular exchange method

To improve the quality of the $CsPbIBr_2$ film, thereby optimizing the performance of solar cells, Zhang's group [149] introduced a simple and feasible method of intermolecular exchange during the preparation of $CsPbIBr_2$, as shown in Fig. 6a. Firstly, CsI and $PbBr_2$ were dissolved in DMSO to form the $CsPbIBr_2$ precursor. After spin-coating the precursor, a transparent $CsPbIBr_2$ film can be formed on a compact substrate [146,150]. In the second step, 50 μL of CsI solution was deposited onto the formed $CsPbIBr_2$ film by the spin-coating method. Since the CsI species has a higher affinity for $PbBr_2$ than DMSO, thus, the intermolecular exchange of CsI and DMSO occurred at the same time in the process of the CsI solution spin-coating [28,35,36]. Finally, after washing with anhydrous isopropyl alcohol and annealing, high quality $CsPbIBr_2$ films can be obtained. The main feature of this method was to spin-coat the optimized CsI methanol solution on the $CsPbIBr_2$ membrane based on the conventional one-step spin-coating method. With merely this step of improvement, the prepared $CsPbIBr_2$ thin film has high phase purity, coverage and crystallinity, uniform particle size, as well as few grain boundaries.

(2) Solvent engineering method

A bilayer architecture that contained mesoscopic and planar structures was obtained by Seok's team [151] *via* the solvent-engineering process. This process that could be used to form uniform and dense perovskite layers, involved five stages. Initially, the mixture of the raw materials and the solvent in an appropriate ratio was spread on the entire surface of the substrate. Then, the spin coater was accelerated to the required rotation speed and held for a certain time to evaporate the solvent. The third key step was to drop a solvent (such as toluene or chloroform) that was miscible with both DMSO and GBL and did not dissolve the perovskite onto the substrate in the process of spinning, as shown in Fig. 6. Fourthly, the residual DMSO was removed and all components were frozen, and then a new complex could be formed as an intermediate phase. Lastly, the composite $CH_3NH_3Pb(I_{1-x}Br_x)_3$ (x=0.1–0.15) was transformed into a highly uniform crystalline perovskite after annealing. The key

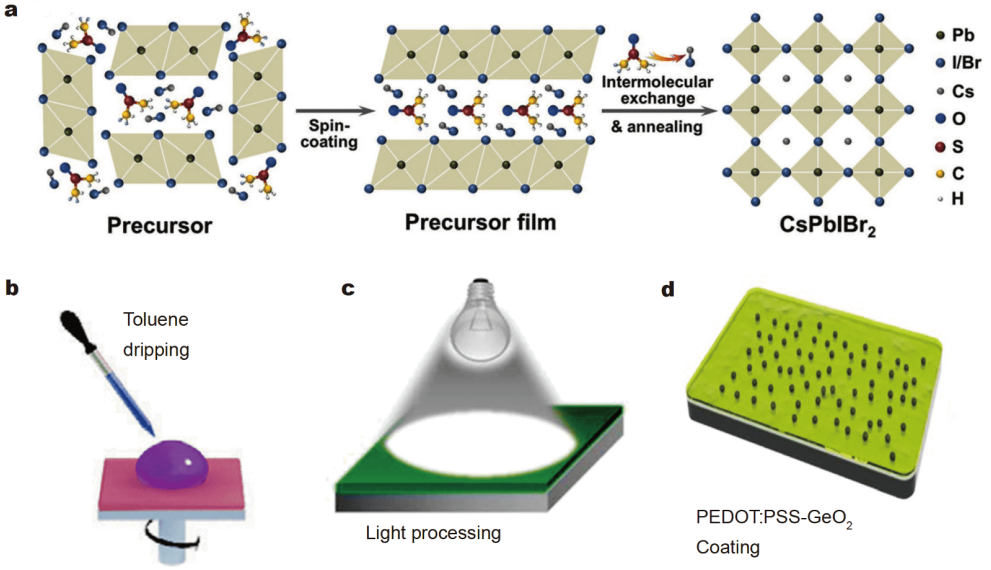

Figure 6 (a) Illustration of intermolecular exchange method. Reprinted with permission from Ref. [149]. Copyright 2018, Wiley. (b) Solvent engineering method. Reprinted with permission from Ref. [151]. Copyright 2014, Springer Nature. (c) Light-processing method. Reprinted with permission from Ref. [73]. Copyright 2019, the American Chemical Society. (d) Seed-mediated growth method. Reprinted with permission from Ref. [152]. Copyright 2016, the American Institute of Physics.

technology of this method was to use a mixed solvent of GBL and DMSO, and then, dropwise add a toluene solvent treatment process to form a uniform and dense intermediate phase of the perovskite layer, which could provide a new way to realize low-cost and highly efficient perovskite solar cells.

(3) Light-processing method

$CsPbIBr_2$ photovoltaic films with preferential orientation, high crystallinity, large size, full coverage, and pure phase were obtained by Zhang's team [73], using a light-processing technology, as shown in Fig. 6c. Initially, the precursor solution containing the raw material $PbBr_2$, CsI, and solvent DMSO was spin-coated on a substrate in a glovebox to form the $CsPbIBr_2$ precursor film. Then, the samples were treated with a simulated one-sun source for 60 min in ambient air atmosphere. The high-quality $CsPbIBr_2$ film was formed after the final annealing treatment. Compared with the film prepared by the conventional method, the obtained film by the light-processing method had a uniform morphology and was pinhole-free.

(4) Seed-mediated growth method

A seed-mediated method by GeO_2 NPs was used to grow high-quality perovskite crystal films reported by Wang's team [152], as shown in Fig. 6d. Firstly, the PEDOT:PSS-GeO_2 composite precursor was spin-coated onto the ITO substrates. GeO_2 NPs of different sizes can be generated by adjusting the doping ratio of GeO_2 and annealing conditions. GeO_2 NPs played the role of the growth point of crystal nucleus, and the perovskite on the bottom layer of substrate started to grow from GeO_2 NPs. Finally, the high-quality perovskite films could be harvested by adjusting the size of GeO_2 NPs onto the substrate. The seed-mediated growth method of perovskite crystals provides a way for seeking other suitable NP materials in the future to make efficient and stable perovskite solar cells. In addition to the methods mentioned above, researchers are also constantly studying new methods, such as the interdiffusion [153] and slot-die coating methods [154], to explore the preparation of high-quality perovskite films for solar cells.

CVD method

CVD is a process widely used in industry, and is one of the many ways demonstrated for the vapor deposition of perovskites. Compared with perovskite films grown by solution, the perovskite materials grown by the CVD method have fewer defects and higher qualities. With the development of perovskite materials grown by CVD, different morphologies, such as platelets, films, micro- and nanowires (NWs), can be grown by controlling the growth conditions. In addition to changing the reaction conditions to obtain perovskite materials with different qualities, researchers also set up different reaction devices to study perovskite crystal materials. Because the growth conditions of organic-inorganic hybrid perovskite materials are quite different from the inorganic perovskite materials, the classification and summary are carried out herein.

Growth of perovskite with different CVD devices

The preparation of organic-inorganic hybrid perovskites and their potential applications mainly depend on the availability of their thin film deposition technology. Organic-inorganic hybrid materials usually cause organic components to decompose or dissociate at a temperature lower than that required for the evaporation of inorganic components during the gradual heating process, which makes it infeasible to prepare organic-inorganic hybrid perovskite materials using the single-source evaporation deposition technology.

In 1998, Mitzi and his coworkers [155] observed that the organic-inorganic hybrid crystals had reassembled in the original hybrid layer during the process of heating and cooling. This observation indicated that if the hybrid material was heated sufficiently fast, it was possible to deposit organic-inorganic thin films using a single evaporation source. Therefore, in 1999, Mitzi and his coworkers [155] used the prototype single source thermal ablation (SSTA) apparatus (Fig. 7a) to prepare several organic-inorganic hybrid perovskites, which included $(C_6H_5C_2H_4NH_3)_2PbI_4$, $(C_6H_5C_2H_4NH_3)_2PbBr_4$, and $(C_4H_9NH_3)_2SnI_4$. These examples showed that the technique can be used in the preparation of a variety of organic-inorganic hybrid perovskites with strong luminescence. In 2013, Snaith's group [62] created uniform flat films of the mixed halide perovskite $CH_3NH_3PbI_{3-x}Cl_x$ by dual-source vapor deposition. Fig. 7b shows an illustration of the vapor-deposition set-up.

With the development of growth methods of perovskite materials, CVD devices have been improved continuously, such that high-quality perovskite materials with different morphologies can be grown. A CVD device with a single source and temperature zone is the most commonly used device for pure inorganic perovskite growth, as shown in Fig. 8a.

Generally, the heated CsX and PbX_2 (X=Cl, Br, I) mixture powder in the heated zone was used to obtain the $CsPbX_3$ (X=Cl, Br, I) ultrathin platelets [156], microspheres [157], oriented NWs and MWs [83], and so on.

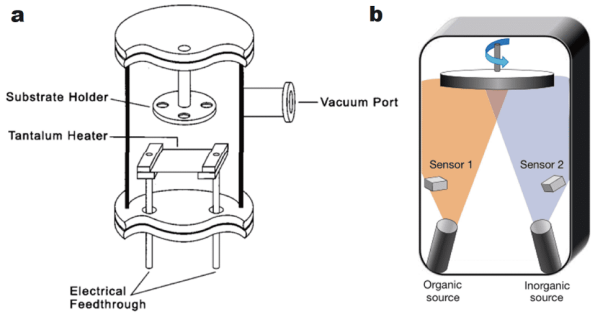

Figure 7 (a) Cross sectional view of a typical single source thermal ablation chamber. Reprinted with permission from Ref. [155]. Copyright 1999, American Chemical Society. (b) Dual-source thermal evaporation system for depositing the perovskite absorbers. Reprinted with permission from Ref. [62]. Copyright 2013, Springer Nature.

For example, Zeng's group [156] used van der Waals epitaxy to grow all-inorganic perovskite $CsPbBr_3$ ultrathin platelets on different substrates to obtain materials with superb qualities. The source was the mixed powder of $PbBr_2$ and CsBr in a molar ratio of 1:1. The mixed source and ultrathin mica were put in a quartz tube in a single zone furnace. The ultrathin mica was placed inside the downstream of the quartz tube. Afterward, high-purity Ar (99.99%) was passed through the tube until the atmospheric pressure reached 10 Pa. Keeping the flow rate of high-purity Ar at 35 sccm, the reaction was conducted under atmospheric pressure. The reaction temperature was increased from room temperature to 575°C within 20 min, and the deposition lasted for 15 min. Then, they obtained the $CsPbX_3$ ultrathin platelets. Jin's team has developed a CVD system equipped with a mass flow controller and pressure control [82]. Using this system, they have grown high-quality horizontally oriented NWs and MWs of $CsPbX_3$ (X=Cl, Br, or I) with high density on mica, as shown in Fig. 8b. This method is simple and versatile. Mica and muscovite mica were used as substrates and placed downstream in the cooling zone. The ground powders of 10 mmol CsX and 10 mmol PbX_2 were mixed together and used as precursors for $CsPbX_3$ and placed at the center of the heating zone. The distance between the precursor and the substrate was approximately 12 cm. Argon gas was used as the carrier gas with a flow rate of 12 sccm and the pressure inside the CVD tube was maintained at 80 mTorr. The temperature of the central heating zone varied with different halogens. The center of the heating zone was set to 300°C for the synthesis of $CsPbI_3$, 325°C for $CsPbBr_3$, and 350°C for $CsPbCl_3$. The temperature at the substrate was approximately 40°C lower than that at the center of the heating zone measured by the thermocouple. According to the desired products, the CVD reactions were carried out from 5 min to up to 20 h, and then, the furnace was cooled down naturally [83].

According to the different melting points of reactants and the desired morphologies of the products, sometimes the preparation of pure inorganic perovskite also needs

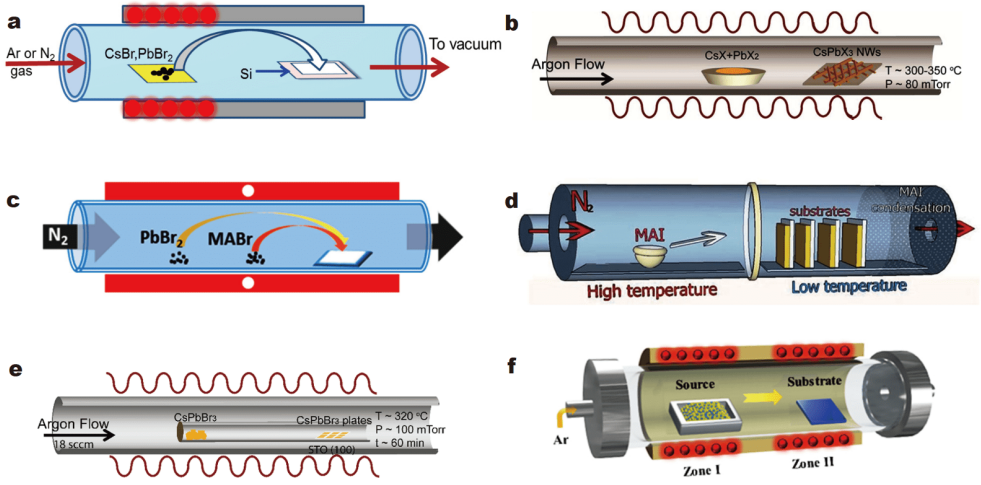

Figure 8 (a) CVD growth diagram of single heat source and single temperature zone [157]. (b) Schematic diagram of CVD to grow $CsPbBr_3$ NWs with single heat source. Reprinted with permission from Ref. [83]. Copyright 2016, the American Chemical Society. (c) Schematic diagram of growing $MAPbBr_3$ using a dual heat source in a single-temperature-zone CVD device. Reprinted with permission from Ref. [76]. Copyright 2019, the American Chemical Society. (d) Diagram of the HCVD furnace and MAI deposition onto metal halide seeded substrates. Reprinted with permission from Ref. [99]. Copyright 2014, the Royal Society of Chemistry. (e) Schematic of growing $CsPbBr_3$ nanoplates on STO substrates with the tube-in-tube setup. Reprinted with permission from Ref. [84]. Copyright 2017, the American Chemical Society. (f) Schematic of growing $CsPbBr_3$ microplatelets with single heat source and dual temperature zone. Reprinted with permission from Ref. [19]. Copyright 2018, the American Chemical Society.

the choices of double sources and single-temperature-zone CVD systems. For example, Shi's group [158] achieved centimeter-scale single-crystalline thin film for inorganic halide perovskites of $CsBBr_3$ (B=Pb, Sn) on a NaCl substrate by vapor phase epitaxy (VPE). The cesium bromide powder (CsBr) was placed in a heating furnace, whose temperature was controlled to approximately 500°C, and lead (II) or tin (II) ($PbBr_2$, $SnBr_2$) was placed in the upper stream approximately 10 cm away from the CsBr owing to its lower melting point. Then, the NaCl substrate was placed approximately 10 cm downstream from the heating zone. The base pressure was controlled to 0.5 Torr before deposition, and then, the flow rate of Argon carrier gas reached 30 sccm, which maintained the pressure at 0.7 Torr before deposition. It only took 7 min to raise the temperature from room temperature to the deposition temperature. According to the thickness of the film before shutting down the furnace, the deposition time can be maintained for 5–20 min. The furnace needed to be cooled to approximately 90°C before removing the NaCl substrate. During the growth process, the NaCl substrate was tilted 45° to ensure uniform coating by the CVD process [158]. Wu's group [76] grew single-crystal platelets of $MAPbBr_3$ on mica substrates by one-step CVD in a single-zone furnace, as shown in Fig. 8c. Square-shaped perovskite platelets were grown on the mica substrate at a pressure of 140 Torr and a growth temperature of 320°C in 20 min. The lateral size of the obtained platelets can reach 10 μm, and their surface is uniform and smooth.

Among many photovoltaic materials, organic-inorganic perovskite films have attracted great attention from researchers due to their good performance in high-efficiency solar cells. Zheng Liu's team cooperated with Xinfeng Liu [77] to explore the growth of perovskite $MAPbI_3$ nanoplatelets on SiO_2/Si substrates by a simple two-step CVD method. As shown in Fig. 8d, highly crystalline PbI_2 nanoplatelets were first grown on the Si/SiO_2 substrate by physical vapor deposition. Then, the PbI_2 crystals were converted into perovskite by the reaction with CH_3NH_3I in vacuum. The size and thickness of the synthesized lead halide perovskite series nanoplatelets can be controlled by adjusting the growth temperature and time of PbI_2 [77]. A new two-step method invented by Qi's team [99], as shown in Fig. 8d, which was used to synthesize perovskite by HCVD, could be easier to prepare and repeat the attainment of high-quality perovskite films. Furthermore, Surya's group [78] conducted an in-depth study. In the first step, a layer of PbX_2 (X=Cl, I, Br), dissolved in DFM solution, was spin-coated onto the substrate. The pre-processed substrate and MAX or FAX (X=Cl, Br, I) were then loaded into two independent temperature-controlled zones of the furnace [159]. But the power of MAX or FAX (X=Cl, Br, I) need to be maintained at T_1, for example, usually T_{MAI}=180°C. The pre-processed substrate was placed downstream to the MAX or FAX (X=Cl, Br, I). The sublimated MAX or FAX (X=Cl, Br, I) was transported by carrier gas to a predetermined area, which crystallized the $MAPbX_3$ or $FAPbX_3$ film. The diffusion of MAX or FAX (X=Cl, Br, I) took place in two phases. In the HCVD method, the MAX or FAX (X=Cl, Br, I) can diffuse into the substrate in gas phase.

To react with the metal halide present on the bottom surface to form a perovskite film, the MAX or FAX (X=Cl, Br, I) must diffuse through the film (i.e., solid diffusion). Surya's team [78] found that higher temperatures could increase the rate of gas and solid diffusion, as well as the rate of perovskite conversion. Multi-region HCVD has independent and precise control over the pressure, carrier gas type, gas flow rate, raw material, and substrate temperature, which helps to improve its reproducibility and perovskite film performance. A new HPCVD method was introduced by Cui's group [96] to synthesize high-quality perovskite films of $CH_3NH_3PbI_3$. Compared with published vapor-based methods, $CH_3NH_3PbI_3$ thin films were synthesized in a well-controlled vacuum and isothermal environment. Critical reaction parameters, including vapor pressure and reaction temperature, can be adjusted accurately to further improve the perovskite film quality. This method is compatible with traditional semiconductor manufacturing methods, and can obtain high-quality perovskite films through accurate process control. Eventually, perovskite-based solar cells can achieve low-cost, large-scale production.

To grow perovskite materials with different morphologies and high qualities, the device for growing perovskite materials is also constantly upgrading and improving. A micrometer-thick $CsPbBr_3$ single-crystal array film was grown on conventional $SrTiO_3$ (100) substrates *via* VPE, which was first reported by Jin's group [84]. The growth of the epitaxial $CsPbBr_3$ nanoplates and single-crystal thin films was carried out in a home-built "tube-in-tube" CVD setup that was equipped with mass flow controllers and pressure control, as shown in Fig. 8e. The inner diameters of the outer and inner tubes are 2.1 and 1.2 cm, respectively. This "tube-in-tube" setup with the sealed end of the inner tube facing the carrier gas flow direction helps to maintain a steady laminar flow in the reactor for controlled growth. Initially, $CsPbBr_3$ ingots were pre-

pared by melting CsBr and $PbBr_2$ (in 1:1 molar ratio) at 550°C under atmosphere pressure, and then used as the precursor for the epitaxial growth. Then the $CsPbBr_3$ ingots were placed at the center of the heating zone inside the inner tube close to the sealed end of the inner tube. The $SrTiO_3$ (100) substrates were placed downstream at the cooling zone closer to the open end of the inner tube. The distance between the precursor and the $SrTiO_3$ (STO) substrate was approximately 12 cm. The pressure of the argon carrier gas inside the CVD tube was maintained at 100 mTorr, and the flow rate of Ar was 18 sccm. For the typical growth of $CsPbBr_3$ nanoplate arrays, the CVD reactions were carried out for 60 min with the center of the heating zone (where the $CsPbBr_3$ precursor was) set to 320°C, as shown in Fig. 8e. For the successful growth of continuous $CsPbBr_3$ single-crystal thin films, the CVD reactions were run at 450°C (the temperature of the precursor) for 12–20 min, depending on the desired thickness. Once the reaction was finished, the furnace was turned off and allowed to cool naturally to room temperature [84].

A dual-temperature zone tube furnace was used as a reactor to synthesize high-quality micrometer-scale inorganic $CsPbBr_3$ microplatelets by Shi's team [19] using the CVD method, as shown in Fig. 8f. According to the molar ratio of 1:2, the CsBr and $PbBr_2$ powders were mixed together and formed the precursors, which were placed in the zone I of the tube furnace and heated to 580°C. The substrate SiO_2/Si was also placed in the zone II of the tube furnace and needed to be heated to 360°C, which was different from that of the single zone furnace. After adjusting the two zones to the predetermined temperature and pressure, and keeping the deposition for 20 min, the $CsPbBr_3$ microplatelets on the SiO_2/Si substrate can be harvested [19].

To remove toxic Pb, perovskite materials based on Sn or Bi cations have also been studied extensively. For example, a CVD reactor developed by Sanders's team [160] can simultaneously deposit solvent-free precursors of MAI and BiI_3 under low vacuum, which was a deposition tool based on the showerhead and was the first application to the growth of perovskite, as shown in Fig. 9. The CVD reactor can provide precise process control, making it possible for large-area production. Nitrogen was used as the protective gas, and the N_2 flow was set to 500 sccm. To avoid cross-contamination, BiI_3 and MAI were placed in two different crucibles to form evaporation sources. According to the MAI/BiI_3 ratio and the crucible filling amount, the BiI_3 crucible needed to be heated to 240–270°C, and the MAI crucible was heated to 180–200°C.

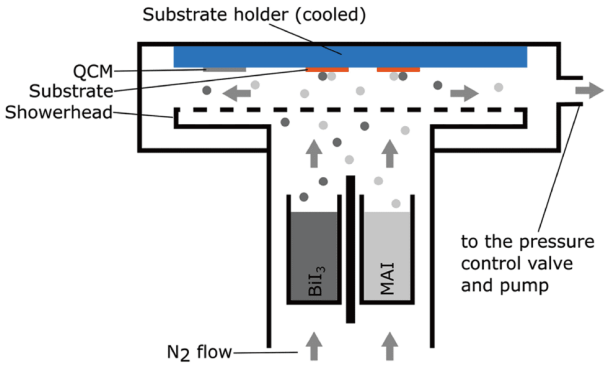

Figure 9 Schematic illustration of showerhead-based deposition tool for the growth of perovskites. Reprinted with permission from Ref. [160]. Copyright 2019, Springer Nature.

Generally, the gas mixture of sublimed molecules and carrier gas be dispersed when the showerhead was maintained at 260°C, such that it could be uniformly deposited on substrates with an area of 108 cm^2 (12 cm×9 cm). They not only studied the effect of precursor velocity on the layer morphology and optical and crystallographic properties by changing the ratio of MAI/BiI_3 precursor, but also investigated the effect of substrate temperature and layer thickness on the morphology of methylammonium bismuth iodide (MBI) crystalline by changing the temperature.

Effect of growth conditions on the morphology of perovskite

With the change of growth conditions (growth temperature, pressure, time, substrate, etc.), perovskite materials with different morphologies, such as triangles, squares, hexagomacro/nanoplatelets [161,76,7], triangular pyramid nanocrystals [85], micro/nanorods [30], NWs with a square end facet [162], nanospheres [157], and nano-array [84], can be grown by the CVD method, as shown in Fig. 10a–h.

Wu's team worked in conjunction with Liu [74] to investigate the effect of the pressure of the carrier gas and temperature of the source on the morphology of $MAPbBr_3$ platelets. Fig. 11a presents the change of crystal morphology with growth conditions. The growth time was kept the same. The square-shaped platelets cannot be obtained at the lower pressure and growth temperature. For example, 3D spheres with a uniform diameter can be observed at 100 Torr and 320°C. Then, the 2D platelets and 3D spheres coexisting can be observed with the increase of pressure (Fig. $11a_2$). With continued pressure increase, the 3D spheres finally disappeared (Fig. $11a_3$), which indicated a transition between the pressure-

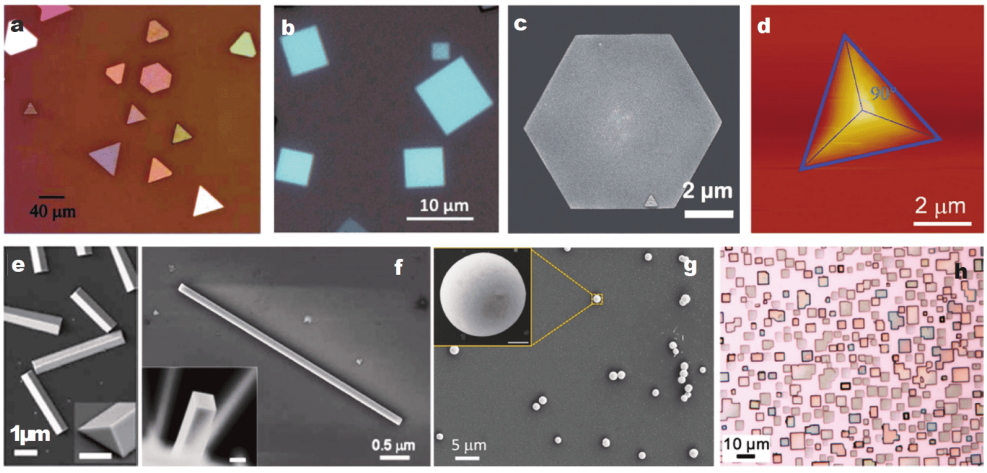

Figure 10 (a) Growth of triangular $MAPbI_3$ nanoplatelets on the mica substrate. Reprinted with permission from Ref. [161]. Copyright 2019, Wiley. (b) Growth of square $MAPbBr_3$ single-crystal platelet. Reprinted with permission from Ref. [76]. Copyright 2019, the American Chemical Society. (c) Growth of hexagonal $MAPbI_3$ nanoplatelets on the Si/SiO_2 substrate. Reprinted with permission from Ref. [77]. Copyright 2016, Wiley. (d) Growth of a typical $MAPbBr_3$ triangular pyramid nanocrystal on a mica substrate. Reprinted with permission from Ref. [85]. Copyright 2018, Wiley. (e) Growth of the $CsPbBr_3$ micro/nanorods. Reprinted with permission from Ref. [30]. Copyright 2016, the American Chemical Society. (f) Growth of a typical nanowire with a square end facet. Reprinted with permission from Ref. [162]. Copyright 2018, Wiley. (g) Growth of the $CsPbBr_3$ microcrystals on the silicon wafer with a spherical shape. Reprinted with permission from Ref. [157]. Copyright 2019, the Royal Society of Chemistry. (h) Growth of $CsPbBr_3$ nanoplates on the STO(100) substrate. Reprinted with permission from Ref. [84]. Copyright 2017, the American Chemical Society.

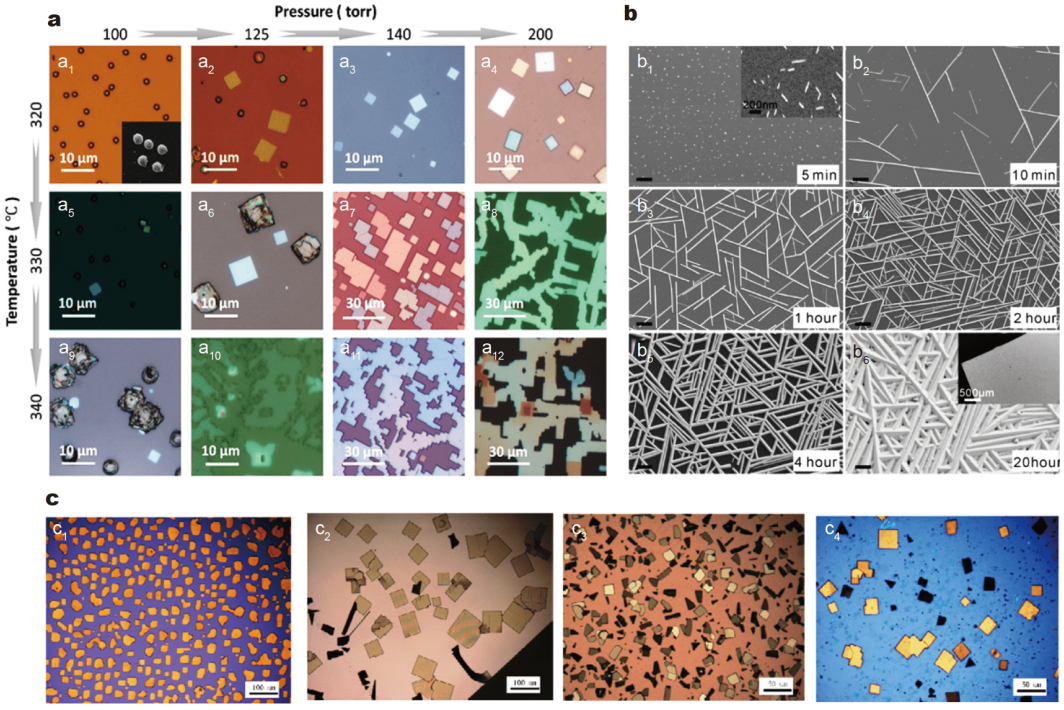

Figure 11 (a) Effects of temperature and pressure on the morphology of perovskite crystals. Reprinted with permission from Ref. [76]. Copyright 2019, the American Chemical Society. (b) Scanning electron microscope (SEM) images of the $CsPbBr_3$ NWs and MWs, networks, and continuous film grown on p-mica with different reaction times from 5 min to 20 h. Reprinted with permission from Ref. [83]. Copyright 2016, the American Chemical Society. (c) Optical images of $CsPbBr_3$ ultrathin platelets on different substrates (c_1) SiO_2/Si, (c_2) GaN, (c_3) FTO glass, (c_4) graphene. Reprinted with permission from Ref. [156]. Copyright 2017, the American Chemical Society.

induced 2D and 3D nucleation modes. At a high pressure of 200 Torr, larger and thicker platelets could be observed, which showed that growth rate was also related to pressure.

The growth temperature also has an important effect on the morphology of the perovskite. Upon increasing the furnace temperature from 320 to 330°C, nearly no platelets can be observed at lower pressure (Fig. 11a_5), and some irregular structures appeared with the pressure increasing to 125 Torr (Fig. 11a_6). When the temperature was kept at 330°C, and the pressure changed, the formation of the larger perovskite structures, which consisted of connected square platelets, could be observed (Fig. 11a_7, a_8). On increasing the temperature further to 340°C (Fig. 11a_9–a_{12}), a similar evolution of the perovskite morphology with that at 330°C was observed, except that the platelets tended to connect together and formed thick terrace structures. Finally, it can be observed the platelets can be broken down into amorphous structures at high growth temperatures and low pressures (e.g., Fig. 11a_5, a_6, a_9, a_{10}) [76].

In cooperation with Wu's group, Mi *et al.* [85] found that the growth temperature had a great effect on the morphology of $MAPbBr_3$ single crystals in the growth process of pyramid-shaped $MAPbBr_3$ by the CVD method, as shown in Fig. 10d. Generally, the center temperature was set at 345°C in the growth process. On slightly increasing the growth temperature (10°C), they found that the top of the pyramids would be flat with some concave cubic corners. When Jin's team [83] used a "tube-in-tube" CVD device to grow $CsPbBr_3$ single crystal thin films, they found that increasing the reaction temperature was the key to realize the continuous growth of $CsPbBr_3$ single crystals. Increasing the temperature not only enhanced the diffusion of adsorbed atoms but also accelerated the nucleation of the preferred epitaxial crystals.

The growth time in CVD also has significant influence on the quality and the morphology of perovskite materials. Jin's group [83] synthesized $CsPbX_3$ (X=Cl, Br, I) NWs and MWs by a modified CVD system. When the deposition time changed from 5 min to 20 h, a variety of $CsPbBr_3$ nanostructures could be obtained, such as single NWs, Y-shaped branches, and interconnected NW or MW networks, as shown in Fig. 11b.

In the growth process of the cube-cornered $CH_3NH_3PbBr_3$ pyramids, Mi *et al.* [85] found that the sizes of the cube-cornered $CH_3NH_3PbBr_3$ pyramids could be controlled accurately with slight deviations in the growth time. When the growth temperature was kept at 345°C, the size of the pyramids increased with the growth time. At a growth time of 15 min, small pyramids with a uniform lateral size of 2 μm can be distinguished. However, with the growth time increasing to 30 min, large pyramids with a lateral size of approximately 10 μm can be found among the small pyramids. Additionally, with a longer growth time, the size distribution would not be as uniform as that with a shorter growth time. The reason could be that smaller pyramids were formed at a later time compared with the larger ones.

The substrate also affects the morphology and quality of the crystal. For example, Zeng's group [156] not only obtained the $CsPbBr_3$ ultrathin platelets on ultrathin mica by the CVD method, but also grew the $CsPbBr_3$ ultrathin platelets on different substrates, including graphene, GaN, FTO glass, and SiO_2/Si, as shown in Fig. 11c. It can be seen from Fig. 11c that the morphologies and qualities of the $CsPbBr_3$ ultrathin platelets are different with various substrates.

The key step in realizing practical optoelectronic devices was to control the growth or patterning of perovskite components on ubiquitous silicon optoelectronic platforms. By pre-patterning a single-layer hexagonal boron nitride (h-BN) buffer layer, Liu's group [163] obtained high-quality patterned perovskite arrays on Si substrate for lasing and light emission *via* a novel bottom-up growth technique, as shown in Fig. 12.

The BN films were synthesized on Cu foil by the CVD method. Initially, the BN films were transferred to the SiO_2/Si substrates in a standard transfer method. Then, using standard photo-lithography methods, the large-area BN film (wafer scale) was patterned. Finally, a single-layer BN film was used as a buffer layer, and a high-quality halide perovskite-type microcrystalline array was prepared on a silicon substrate by a two-step CVD method. It can be seen that the quality and morphology of perovskite materials are greatly affected by the growth device, growth conditions, and growth process. Therefore, to prepare perovskite materials with different morphologies and halides, the required conditions will be different.

Xiong's group [31,164] synthesized high-quality crystalline $CH_3NH_3PbI_3$, $CH_3NH_3PbBr_3$, $CH_3NH_3PbCl_3$, $CH_3NH_3PbI_xCl_{3-x}$, $CH_3NH_3PbI_xBr_{3-x}$, and $CH_3NH_3PbBr_xCl_{3-x}$ platelets and NWs by adjusting the precursor, reaction temperature, and pressure *via* a two-step vapor phase method. Firstly, PbX_2 (X=I, Br, or Cl) platelets or NWs were prepared on mica substrate by the CVD method. Secondly, using PbX_2/CH_3NH_3X (X=I, Br, or Cl) as the reaction precursor, the organic-inorganic hybrid per-

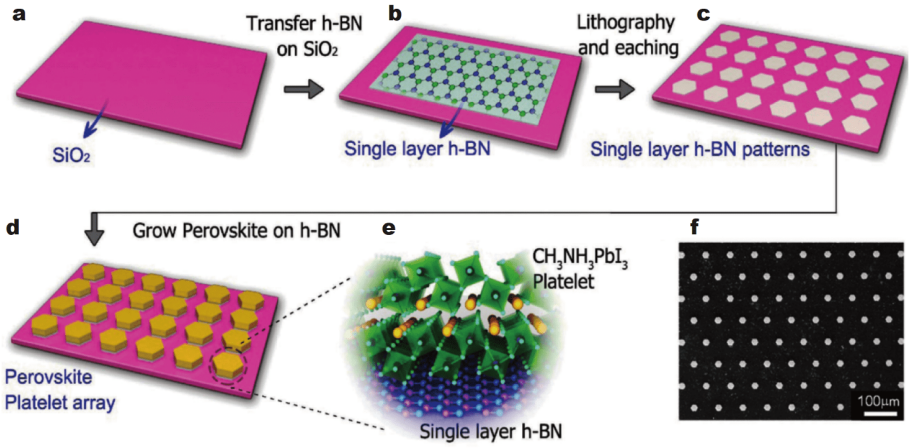

Figure 12 Fabrication process for the perovskite platelet array and SEM image of the as-prepared $CH_3NH_3PbX_3$ (X=Cl, Br, I) platelet array. Reprinted with permission from Ref. [163]. Copyright 2016, Wiley.

ovskite was prepared by the CVD method with Ar or N_2 as the protective gas. However, for the synthesis of PbX_2, the mica substrate needed to be put in the downstream zone of the quartz tube. Furthermore, the CH_3NH_3X (X=I, Br, or Cl), prepared by a solution method, was used as a source, and it needed to be placed in the center of the quartz tube, while the silicon wafer also had to be placed in the downstream region. Then, a similar CVD system was used to prepare the CH_3NH_3PbX (X=I, Br, or Cl) NWs. Different halogens and crystal morphologies need different preparation temperatures and pressures [31,164]. The different specific preparation conditions are shown in Table 2.

Compared with organic-inorganic hybrid perovskites, the solubility of inorganic perovskites is lower. For example, the Cs-Pb-X phase diagram is more complicated, with three phases of $CsPbBr_3$, $CsPb_2Br_5$, and Cs_4PbBr_6, such that the solution method used to grow inorganic perovskites is usually more difficult [66–68]. Therefore, there was an urgent need to develop an effective method to grow inorganic halide perovskite materials [84]. Xiong's [32], Jin's [83,84], Zhang's [75], and Liu's [74,157,162] groups have done a lot of work on the growth of inorganic perovskite. For example, they prepared high-quality single-crystalline $CsPbX_3$ (X=Cl, Br, I) perovskite nanoplatelets on a muscovite mica substrate by a modified CVD system [32]. The detailed reaction conditions are shown in Table 3.

Through the change of growth conditions and devices, various perovskite materials with different morphologies can be grown by CVD, such as platelets, square sheets, triangular sheets, micro/nanowires, pyramids and micro/nano spheres. Therefore, the CVD method can be used to grow high-quality perovskite materials with specific morphologies, according to the actual needs.

CONCLUSIONS AND OUTLOOK

The unique and excellent properties of metal halide perovskites, such as extended diffusion lengths, long carrier lifetimes, high wavelength tenability, high fluor-

Table 2 The preparation conditions of $MAPbX_3$

First-step					Second-step					Ref.
Product	Protective gas	T (°C)	P (Torr)	Time (min)	Product	Protective gas	T (°C)	P (Torr)	Time (min)	
PbI_2 platelet	High-purity H_2/Ar (5:9, v/v)	380	200	20	$MAPbI_3$ platelets	High-purity Ar or N_2 gas	115	40	60	[31]
$PbBr_2$ platelets		350	75	20	$MAPbBr_3$ platelets					[31]
$PbCl_2$ platelets		510	200	20	$MAPbCl_3$ platelets					[31]
PbI_2 NWs		380	200	15	$MAPbI_3$ NWs	High-purity N_2 gas	120	50	60	[164]
$PbBr_2$ NWs		350	50	15	$MAPbBr_3$ NWs					[164]
$PbCl_2$ NWs					$MAPbCl_3$ NWs		100			[164]

Table 3 The preparation conditions of $CsPbX_3$

Crystal morphology	Substrate	The ratio of precursor	Protective gas/rate of flow	T (°C)	P (Torr)	Time (min)	Ref.
$CsPbCl_3$ nanoplatelets	Muscovite mica	$PbCl_2$/CsCl=1:1	High-purity N_2 (30 sccm)	625	100		[32]
$CsPbBr_3$ nanoplatelets		$PbBr_2$/CsBr=1:1		575	50		[32]
$CsPbI_3$ nanoplatelets		PbI_2/CsI=1:1		550	100	20	[32]
$CsPbCl_3$ NWs		$PbCl_2$/CsCl=1:1	High-purity N_2 gas	620	100		[75]
$CsPbBr_3$ NWs		$PbBr_2$/CsBr=1:1		575	50		[75]
$CsPbBr_3$ NWs	Si	$PbBr_2$/CsBr=1:2	High-purity Ar (90 sccm)	570	400	15	[162]
$CsPbBr_3$ MWs/NWs		$PbBr_2$/CsBr=1:1	High-purity N_2 (30 sccm)	575	100	10	[74]
$CsPbBr_3$ microspheres		$PbBr_2$/CsBr=1:2	High-purity Ar gas	575	–	–	[157]

escence yields, and high light-absorption regions, contribute to their good application prospects in the field of lasers, photodetectors, X-ray detectors, γ-ray detectors, solar cells, p-light emitting diodes (LEDs), and so on. The quality of the metal halide is the key to the application of metal halide perovskites, and the growth technology has a significant impact on the material quality. Therefore, the research progress of several main methods for growing perovskite materials in recent years include the STL, ITC, AVC, spin-coating, and CVD methods. The STL, ITC, and AVC methods are usually used to grow large-sized bulk single crystals of perovskite. Although the STL method is more time-consuming, it can grow high-quality large-scale bulk single crystals. The ITC method not only depends on the temperature of the solution but also requires stronger solvents. For example, DMF, DMSO, and GBA are the common solvents used in the ITC method. The solvents are generally different when the halogens vary in the perovskite single crystals. Single-crystal perovskites can be grown rapidly by the AVC method, but the proper anti-solvent should be selected. In the AVC method, dichloromethane, toluene, ether, and ethanol are commonly used as anti-solvents. The spin-coating method is mainly used to prepare high-performance polycrystalline or microcrystalline perovskite films for solar cells. However, the spin-coating method has some limitations in the preparation of large-area perovskite films. The CVD method can be used to grow large-area perovskite films by changing the growth device through the modification of the growth conditions; thus, perovskites with different morphologies, such as thin film, micro/nano platelet, NWs, and micro/nano sphere, can be prepared *via* the CVD method.

Although the methods of crystal growth are classified, two or three methods are often used together for growing high-quality single crystals. For example, the reported modified ITC method to grow $FAPbI_3$ single crystals by Yang's group [56] included the STL and the ITC methods. Additionally, the reported HCVD method by Qi's group [99] included the spin-coating and the CVD methods. Therefore, to grow high-quality perovskite materials, the exploration of growth processes needs to continue. In addition, the toxicity of lead in perovskites has limited their commercial developments and applications. Therefore, it is more practical to study the growth and the associated methods of lead-free perovskites in the future. However, currently, it is difficult to commercialize the growth of perovskites. In the future, it will be necessary to explore low-cost, environmentally friendly, and convenient preparation methods of perovskite materials, which are also the necessitated conditions for the commercialization of perovskite materials.

Received 6 January 2020; accepted 14 March 2020; published online 3 June 2020

1 Liu Y, Yang Z, Liu SF. Recent progress in single-crystalline perovskite research including crystal preparation, property evaluation, and applications. Adv Sci, 2018, 5: 1700471
2 Møller CK. Crystal structure and photoconductivity of cæsium plumbohalides. Nature, 1958, 182: 1436
3 Haque MA, Sheikh AD, Guan X, *et al.* Metal oxides as efficient charge transporters in perovskite solar cells. Adv Energy Mater, 2017, 7: 1602803
4 Liu Z, Mi Y, Guan X, *et al.* Morphology-tailored halide perovskite platelets and wires: from synthesis, properties to optoelectronic devices. Adv Opt Mater, 2018, 6: 1800413
5 Weber D. $CH_3NH_3PbX_3$, ein Pb(II)-system mit kubischer perowskitstruktur/$CH_3NH_3PbX_3$, a Pb(II)-system with cubic perovskite structure. Z für Naturforschung B, 1978, 33: 1443–1445
6 Weber D. $CH_3NH_3SnBr_xI_{3-x}$ (x=0–3), ein Sn(II)-system mit kubischer perowskitstruktur/$CH_3NH_3SnBr_xI_{3-x}$ (x=0–3), a Sn(II)-system with cubic perovskite structure. Z für Naturforschung B, 1978, 33: 862–865

7 Kojima A, Teshima K, Shirai Y, *et al.* Organometal halide perovskites as visible-light sensitizers for photovoltaic cells. J Am Chem Soc, 2009, 131: 6050–6051
8 Dong R, Fang Y, Chae J, *et al.* High-gain and low-driving-voltage photodetectors based on organolead triiodide perovskites. Adv Mater, 2015, 27: 1912–1918
9 Zhang X, Sun C, Zhang Y, *et al.* Bright perovskite nanocrystal films for efficient light-emitting devices. J Phys Chem Lett, 2016, 7: 4602–4610
10 Stranks SD, Eperon GE, Grancini G, *et al.* Electron-hole diffusion lengths exceeding 1 micrometer in an organometal trihalide perovskite absorber. Science, 2013, 342: 341–344
11 Wehrenfennig C, Eperon GE, Johnston MB, *et al.* High charge carrier mobilities and lifetimes in organolead trihalide perovskites. Adv Mater, 2014, 26: 1584–1589
12 Jeon NJ, Noh JH, Yang WS, *et al.* Compositional engineering of perovskite materials for high-performance solar cells. Nature, 2015, 517: 476–480
13 Park NG. Perovskite solar cells: an emerging photovoltaic technology. Mater Today, 2015, 18: 65–72
14 Liu Y, Yang Z, Cui D, *et al.* Two-inch-sized perovskite $CH_3NH_3PbX_3$ (X=Cl, Br, I) crystals: growth and characterization. Adv Mater, 2015, 27: 5176–5183
15 Liu D, Wang Q, Traverse CJ, *et al.* Impact of ultrathin C_{60} on perovskite photovoltaic devices. ACS Nano, 2018, 12: 876–883
16 Sutherland BR, Sargent EH. Perovskite photonic sources. Nat Photon, 2016, 10: 295–302
17 Zhang Y, Liu Y, Li Y, *et al.* Perovskite $CH_3NH_3Pb(Br_xI_{1-x})_3$ single crystals with controlled composition for fine-tuned bandgap towards optimized optoelectronic applications. J Mater Chem C, 2016, 4: 9172–9178
18 Murali B, Saidaminov MI, Abdelhady AL, *et al.* Robust and air-stable sandwiched organo-lead halide perovskites for photodetector applications. J Mater Chem C, 2016, 4: 2545–2552
19 Li Y, Shi Z, Lei L, *et al.* Highly stable perovskite photodetector based on vapor-processed micrometer-scale $CsPbBr_3$ microplatelets. Chem Mater, 2018, 30: 6744–6755
20 Tiep NH, Ku Z, Fan HJ. Recent advances in improving the stability of perovskite solar cells. Adv Energy Mater, 2016, 6: 1501420
21 Liang J, Wang C, Wang Y, *et al.* All-inorganic perovskite solar cells. J Am Chem Soc, 2016, 138: 15829–15832
22 Chen Q, Zhou H, Fang Y, *et al.* The optoelectronic role of chlorine in $CH_3NH_3PbI_3$(Cl)-based perovskite solar cells. Nat Commun, 2015, 6: 7269
23 Jiang Q, Zhang L, Wang H, *et al.* Enhanced electron extraction using SnO_2 for high-efficiency planar-structure $HC(NH_2)_2PbI_3$-based perovskite solar cells. Nat Energy, 2017, 2: 16177
24 Gao F, Zhao Y, Zhang X, *et al.* Recent progresses on defect passivation toward efficient perovskite solar cells. Adv Energy Mater, 2020, 10: 1902650
25 Wang P, Zhang X, Zhou Y, *et al.* Solvent-controlled growth of inorganic perovskite films in dry environment for efficient and stable solar cells. Nat Commun, 2018, 9: 2225
26 Zhou H, Chen Q, Li G, *et al.* Interface engineering of highly efficient perovskite solar cells. Science, 2014, 345: 542–546
27 You J, Hong Z, Yang YM, *et al.* Low-temperature solution-processed perovskite solar cells with high efficiency and flexibility. ACS Nano, 2014, 8: 1674–1680
28 Guo Y, Yin X, Liu J, *et al.* Highly efficient $CsPbIBr_2$ perovskite solar cells with efficiency over 9.8% fabricated using a preheating-assisted spin-coating method. J Mater Chem A, 2019, 7: 19008–19016
29 Li M, Wei Q, Muduli SK, *et al.* Enhanced exciton and photon confinement in ruddlesden-popper perovskite microplatelets for highly stable low-threshold polarized lasing. Adv Mater, 2018, 30: 1707235
30 Zhou H, Yuan S, Wang X, *et al.* Vapor growth and tunable lasing of band gap engineered cesium lead halide perovskite micro/nanorods with triangular cross section. ACS Nano, 2016, 11: 1189–1195
31 Zhang Q, Ha ST, Liu X, *et al.* Room-temperature near-infrared high-q perovskite whispering-gallery planar nanolasers. Nano Lett, 2014, 14: 5995–6001
32 Zhang Q, Su R, Liu X, *et al.* High-quality whispering-gallery-mode lasing from cesium lead halide perovskite nanoplatelets. Adv Funct Mater, 2016, 26: 6238–6245
33 Chen J, Du W, Shi J, *et al.* Perovskite quantum dot lasers. InfoMat, 2020, 2: 170–183
34 Ling Y, Tian Y, Wang X, *et al.* Enhanced optical and electrical properties of polymer-assisted all-inorganic perovskites for light-emitting diodes. Adv Mater, 2016, 28: 8983–8989
35 Yantara N, Bhaumik S, Yan F, *et al.* Inorganic halide perovskites for efficient light-emitting diodes. J Phys Chem Lett, 2015, 6: 4360–4364
36 Li G, Rivarola FWR, Davis NJLK, *et al.* Highly efficient perovskite nanocrystal light-emitting diodes enabled by a universal cross-linking method. Adv Mater, 2016, 28: 3528–3534
37 Jin X, Zhang X, Fang H, *et al.* Facile assembly of high-quality organic-inorganic hybrid perovskite quantum dot thin films for bright light-emitting diodes. Adv Funct Mater, 2018, 28: 1705189
38 Wei Q, Li M, Zhang Z, *et al.* Efficient recycling of trapped energies for dual-emission in mn-doped perovskite nanocrystals. Nano Energy, 2018, 51: 704–710
39 Cao Y, Wang N, Tian H, *et al.* Perovskite light-emitting diodes based on spontaneously formed submicrometre-scale structures. Nature, 2018, 562: 249–253
40 Wang J, Wang N, Jin Y, *et al.* Interfacial control toward efficient and low-voltage perovskite light-emitting diodes. Adv Mater, 2015, 27: 2311–2316
41 Wang N, Cheng L, Ge R, *et al.* Perovskite light-emitting diodes based on solution-processed self-organized multiple quantum wells. Nat Photon, 2016, 10: 699–704
42 Lai ML, Tay TYS, Sadhanala A, *et al.* Tunable near-infrared luminescence in tin halide perovskite devices. J Phys Chem Lett, 2016, 7: 2653–2658
43 Swarnkar A, Chulliyil R, Ravi VK, *et al.* Colloidal $CsPbBr_3$ perovskite nanocrystals: luminescence beyond traditional quantum dots. Angew Chem Int Ed, 2015, 54: 15424–15428
44 Pan W, Wu H, Luo J, *et al.* $Cs_2AgBiBr_6$ single-crystal X-ray detectors with a low detection limit. Nat Photon, 2017, 11: 726–732
45 Saidaminov MI, Haque MA, Savoie M, *et al.* Perovskite photodetectors operating in both narrowband and broadband regimes. Adv Mater, 2016, 28: 8144–8149
46 Sun Z, Aigouy L, Chen Z. Plasmonic-enhanced perovskite-graphene hybrid photodetectors. Nanoscale, 2016, 8: 7377–7383
47 Lu J, Sheng X, Tong G, *et al.* Ultrafast solar-blind ultraviolet detection by inorganic perovskite $CsPbX_3$ quantum dots radial junction architecture. Adv Mater, 2017, 29: 1700400
48 Tong G, Geng X, Yu Y, *et al.* Rapid, stable and self-powered

perovskite detectors *via* a fast chemical vapor deposition process. RSC Adv, 2017, 7: 18224–18230
49 Li Y, Shi Z, Lei L, *et al.* Controllable vapor-phase growth of inorganic perovskite microwire networks for high-efficiency and temperature-stable photodetectors. ACS Photonics, 2018, 5: 2524–2532
50 Ding J, Fang H, Lian Z, *et al.* A self-powered photodetector based on a $CH_3NH_3PbI_3$ single crystal with asymmetric electrodes. CrystEngComm, 2016, 18: 4405–4411
51 Gao L, Zeng K, Guo J, *et al.* Passivated single-crystalline $CH_3NH_3PbI_3$ nanowire photodetector with high detectivity and polarization sensitivity. Nano Lett, 2016, 16: 7446–7454
52 Deng H, Dong D, Qiao K, *et al.* Growth, patterning and alignment of organolead iodide perovskite nanowires for optoelectronic devices. Nanoscale, 2015, 7: 4163–4170
53 Li J, Yuan S, Tang G, *et al.* High-performance, self-powered photodetectors based on perovskite and graphene. ACS Appl Mater Interfaces, 2017, 9: 42779–42787
54 Liu Y, Zhang Y, Yang Z, *et al.* Thinness- and shape-controlled growth for ultrathin single-crystalline perovskite wafers for mass production of superior photoelectronic devices. Adv Mater, 2016, 28: 9204–9209
55 Liu Y, Sun J, Yang Z, *et al.* 20-mm-large single-crystalline formamidinium-perovskite wafer for mass production of integrated photodetectors. Adv Opt Mater, 2016, 4: 1829–1837
56 Deng H, Yang X, Dong D, *et al.* Flexible and semitransparent organolead triiodide perovskite network photodetector arrays with high stability. Nano Lett, 2015, 15: 7963–7969
57 Chen Q, Wu J, Ou X, *et al.* All-inorganic perovskite nanocrystal scintillators. Nature, 2018, 561: 88–93
58 Luo Q, Ma H, Zhang Y, *et al.* Cross-stacked superaligned carbon nanotube electrodes for efficient hole conductor-free perovskite solar cells. J Mater Chem A, 2016, 4: 5569–5577
59 Liu T, Wang C, Hou J, *et al.* Enhanced electron collection in perovskite solar cells employing thermoelectric $NaCo_2O_4/TiO_2$ coaxial nanofibers. Small, 2016, 12: 5146–5152
60 Luo Q, Zhang Y, Liu C, *et al.* Iodide-reduced graphene oxide with dopant-free spiro-ometad for ambient stable and high-efficiency perovskite solar cells. J Mater Chem A, 2015, 3: 15996–16004
61 Chen Q, Zhou H, Hong Z, *et al.* Planar heterojunction perovskite solar cells *via* vapor-assisted solution process. J Am Chem Soc, 2013, 136: 622–625
62 Liu M, Johnston MB, Snaith HJ. Efficient planar heterojunction perovskite solar cells by vapour deposition. Nature, 2013, 501: 395–398
63 Burschka J, Pellet N, Moon SJ, *et al.* Sequential deposition as a route to high-performance perovskite-sensitized solar cells. Nature, 2013, 499: 316–319
64 Dang Y, Liu Y, Sun Y, *et al.* Bulk crystal growth of hybrid perovskite material $CH_3NH_3PbI_3$. CrystEngComm, 2015, 17: 665–670
65 Lian Z, Yan Q, Gao T, *et al.* Perovskite $CH_3NH_3PbI_3$(Cl) single crystals: rapid solution growth, unparalleled crystalline quality, and low trap density toward 10^8 cm^{-3}. J Am Chem Soc, 2016, 138: 9409–9412
66 Ling Y, Tan L, Wang X, *et al.* Composite perovskites of cesium lead bromide for optimized photoluminescence. J Phys Chem Lett, 2017, 8: 3266–3271
67 Rakita Y, Kedem N, Gupta S, *et al.* Low-temperature solution-grown $CsPbBr_3$ single crystals and their characterization. Cryst Growth Des, 2016, 16: 5717–5725
68 Saidaminov MI, Haque MA, Almutlaq J, *et al.* Inorganic lead halide perovskite single crystals: phase-selective low-temperature growth, carrier transport properties, and self-powered photodetection. Adv Opt Mater, 2017, 5: 1600704
69 Cho H, Jeong SH, Park MH, *et al.* Overcoming the electroluminescence efficiency limitations of perovskite light-emitting diodes. Science, 2015, 350: 1222–1225
70 Li C, Han C, Zhang Y, *et al.* Enhanced photoresponse of self-powered perovskite photodetector based on ZnO nanoparticles decorated $CsPbBr_3$ films. Sol Energy Mater Sol Cells, 2017, 172: 341–346
71 Liu X, Tan X, Liu Z, *et al.* Boosting the efficiency of carbon-based planar $CsPbBr_3$ perovskite solar cells by a modified multistep spin-coating technique and interface engineering. Nano Energy, 2019, 56: 184–195
72 Wang Q, Zheng X, Deng Y, *et al.* Stabilizing the α-phase of $CsPbI_3$ perovskite by sulfobetaine zwitterions in one-step spin-coating films. Joule, 2017, 1: 371–382
73 Zhang Q, Zhu W, Chen D, *et al.* Light processing enables efficient carbon-based, all-inorganic planar $CsPbIBr_2$ solar cells with high photovoltages. ACS Appl Mater Interfaces, 2019, 11: 2997–3005
74 Du W, Zhang S, Shi J, *et al.* Strong exciton-photon coupling and lasing behavior in all-inorganic $CsPbBr_3$ micro/nanowire Fabry-Pérot cavity. ACS Photonics, 2018, 5: 2051–2059
75 Gao Y, Zhao L, Shang Q, *et al.* Ultrathin $CsPbX_3$ nanowire arrays with strong emission anisotropy. Adv Mater, 2018, 30: 1801805
76 Liu Z, Li Y, Guan X, *et al.* One-step vapor-phase synthesis and quantum-confined exciton in single-crystal platelets of hybrid halide perovskites. J Phys Chem Lett, 2019, 10: 2363–2371
77 Niu L, Zeng Q, Shi J, *et al.* Controlled growth and reliable thickness-dependent properties of organic-inorganic perovskite platelet crystal. Adv Funct Mater, 2016, 26: 5263–5270
78 Ng A, Ren Z, Shen Q, *et al.* Crystal engineering for low defect density and high efficiency hybrid chemical vapor deposition grown perovskite solar cells. ACS Appl Mater Interfaces, 2016, 8: 32805–32814
79 Ding J, Yan Q. Progress in organic-inorganic hybrid halide perovskite single crystal: growth techniques and applications. Sci China Mater, 2017, 60: 1063–1078
80 Wang Y, Chang S, Chen X, *et al.* Rapid growth of halide perovskite single crystals: from methods to optimization control. Chin J Chem, 2019, 37: 616–629
81 Fu Y, Rea MT, Chen J, *et al.* Selective stabilization and photophysical properties of metastable perovskite polymorphs of $CsPbI_3$ in thin films. Chem Mater, 2017, 29: 8385–8394
82 Zeng J, Zhou H, Liu R, *et al.* Combination of solution-phase process and halide exchange for all-inorganic, highly stable $CsPbBr_3$ perovskite nanowire photodetector. Sci China Mater, 2019, 62: 65–73
83 Chen J, Fu Y, Samad L, *et al.* Vapor-phase epitaxial growth of aligned nanowire networks of cesium lead halide perovskites ($CsPbX_3$, X=Cl, Br, I). Nano Lett, 2016, 17: 460–466
84 Chen J, Morrow DJ, Fu Y, *et al.* Single-crystal thin films of cesium lead bromide perovskite epitaxially grown on metal oxide perovskite ($SrTiO_3$). J Am Chem Soc, 2017, 139: 13525–13532
85 Mi Y, Liu Z, Shang Q, *et al.* Fabry-Pérot oscillation and room temperature lasing in perovskite cube-corner pyramid cavities. Small, 2018, 14: 1703136
86 Zhang Y, Liu Y, Yang Z, *et al.* High-quality perovskite $MAPbI_3$

single crystals for broad-spectrum and rapid response integrate photodetector. J Energy Chem, 2018, 27: 722–727
87 Liu X, Liu Y, Gao F, *et al.* Photoinduced surface voltage mapping study for large perovskite single crystals. Appl Phys Lett, 2016, 108: 181604
88 Dang Y, Ju D, Wang L, *et al.* Recent progress in the synthesis of hybrid halide perovskite single crystals. CrystEngComm, 2016, 18: 4476–4484
89 Li S, Zhang C, Song JJ, *et al.* Metal halide perovskite single crystals: from growth process to application. Crystals, 2018, 8: 220
90 Babu R, Giribabu L, Singh SP. Recent advances in halide-based perovskite crystals and their optoelectronic applications. Cryst Growth Des, 2018, 18: 2645–2664
91 Saidaminov MI, Abdelhady AL, Murali B, *et al.* High-quality bulk hybrid perovskite single crystals within minutes by inverse temperature crystallization. Nat Commun, 2015, 6: 7586
92 Eperon GE, Burlakov VM, Docampo P, *et al.* Morphological control for high performance, solution-processed planar heterojunction perovskite solar cells. Adv Funct Mater, 2014, 24: 151–157
93 Im JH, Jang IH, Pellet N, *et al.* Growth of $CH_3NH_3PbI_3$ cuboids with controlled size for high-efficiency perovskite solar cells. Nat Nanotech, 2014, 9: 927–932
94 Tavakoli MM, Gu L, Gao Y, *et al.* Fabrication of efficient planar perovskite solar cells using a one-step chemical vapor deposition method. Sci Rep, 2015, 5: 14083
95 Wang B, Chen T. Exceptionally stable $CH_3NH_3PbI_3$ films in moderate humid environmental condition. Adv Sci, 2016, 3: 1500262
96 Peng Y, Jing G, Cui T. A hybrid physical-chemical deposition process at ultra-low temperatures for high-performance perovskite solar cells. J Mater Chem A, 2015, 3: 12436–12442
97 Luo P, Liu Z, Xia W, *et al.* Chlorine-conducted defect repairment and seed crystal-mediated vapor growth process for controllable preparation of efficient and stable perovskite solar cells. J Mater Chem A, 2015, 3: 22949–22959
98 Luo P, Liu Z, Xia W, *et al.* A simple *in situ* tubular chemical vapor deposition processing of large-scale efficient perovskite solar cells and the research on their novel roll-over phenomenon in *J-V* curves. J Mater Chem A, 2015, 3: 12443–12451
99 Leyden MR, Ono LK, Raga SR, *et al.* High performance perovskite solar cells by hybrid chemical vapor deposition. J Mater Chem A, 2014, 2: 18742–18745
100 Leyden MR, Lee MV, Raga SR, *et al.* Large formamidinium lead trihalide perovskite solar cells using chemical vapor deposition with high reproducibility and tunable chlorine concentrations. J Mater Chem A, 2015, 3: 16097–16103
101 Luo P, Liu Z, Xia W, *et al.* Uniform, stable, and efficient planar-heterojunction perovskite solar cells by facile low-pressure chemical vapor deposition under fully open-air conditions. ACS Appl Mater Interfaces, 2015, 7: 2708–2714
102 Leyden MR, Jiang Y, Qi Y. Chemical vapor deposition grown formamidinium perovskite solar modules with high steady state power and thermal stability. J Mater Chem A, 2016, 4: 13125–13132
103 Dong Q, Fang Y, Shao Y, *et al.* Electron-hole diffusion lengths >175 μm in solution-grown $CH_3NH_3PbI_3$ single crystals. Science, 2015, 347: 967–970
104 Zhang H, Liu X, Dong J, *et al.* Centimeter-sized inorganic lead halide perovskite $CsPbBr_3$ crystals grown by an improved solution method. Cryst Growth Des, 2017, 17: 6426–6431
105 Saidaminov MI, Abdelhady AL, Maculan G, *et al.* Retrograde solubility of formamidinium and methylammonium lead halide perovskites enabling rapid single crystal growth. Chem Commun, 2015, 51: 17658–17661
106 Shi D, Adinolfi V, Comin R, *et al.* Low trap-state density and long carrier diffusion in organolead trihalide perovskite single crystals. Science, 2015, 347: 519–522
107 Mitzi DB, Feild CA, Schlesinger Z, *et al.* Transport, optical, and magnetic properties of the conducting halide perovskite $CH_3NH_3SnI_3$. J Solid State Chem, 1995, 114: 159–163
108 Lian Z, Yan Q, Lv Q, *et al.* High-performance planar-type photodetector on (100) facet of $MAPbI_3$ single crystal. Sci Rep, 2015, 5: 16563
109 Chae J, Dong Q, Huang J, *et al.* Chloride incorporation process in $CH_3NH_3PbI_{3-x}Cl_x$ perovskites *via* nanoscale bandgap maps. Nano Lett, 2015, 15: 8114–8121
110 Su J, Chen DP, Lin CT. Growth of large $CH_3NH_3PbX_3$ (X=I, Br) single crystals in solution. J Cryst Growth, 2015, 422: 75–79
111 Xu Z, Li H, Zhao H, *et al.* Optimizing optoelectronic performances by controlling halide compositions of $MAPb(Cl_xI_{1-x})_3$ single crystals. CrystEngComm, 2019, 21: 4169–4174
112 Dang Y, Zhong C, Zhang G, *et al.* Crystallographic investigations into properties of acentric hybrid perovskite single crystals $NH(CH_3)_3SnX_3$ (X=Cl, Br). Chem Mater, 2016, 28: 6968–6974
113 Han Q, Bae SH, Sun P, *et al.* Single crystal formamidinium lead iodide ($FAPbI_3$): insight into the structural, optical, and electrical properties. Adv Mater, 2016, 28: 2253–2258
114 Huang Y, Li L, Liu Z, *et al.* The intrinsic properties of $FA_{(1-x)}MA_xPbI_3$ perovskite single crystals. J Mater Chem A, 2017, 5: 8537–8544
115 Dang Y, Zhou Y, Liu X, *et al.* Formation of hybrid perovskite tin iodide single crystals by top-seeded solution growth. Angew Chem Int Ed, 2016, 55: 3447–3450
116 Dirin DN, Cherniukh I, Yakunin S, *et al.* Solution-grown $CsPbBr_3$ perovskite single crystals for photon detection. Chem Mater, 2016, 28: 8470–8474
117 Liu Y, Ren X, Zhang J, *et al.* 120 mm single-crystalline perovskite and wafers: towards viable applications. Sci China Chem, 2017, 60: 1367–1376
118 Yang Y, Yan Y, Yang M, *et al.* Low surface recombination velocity in solution-grown $CH_3NH_3PbBr_3$ perovskite single crystal. Nat Commun, 2015, 6: 7961
119 Fang HH, Adjokatse S, Wei H, *et al.* Ultrahigh sensitivity of methylammonium lead tribromide perovskite single crystals to environmental gases. Sci Adv, 2016, 2: e1600534
120 Liao Q, Hu K, Zhang H, *et al.* Perovskite microdisk microlasers self-assembled from solution. Adv Mater, 2015, 27: 3405–3410
121 Chen F, Xu C, Xu Q, *et al.* Structure evolution of $CH_3NH_3PbBr_3$ single crystal grown in *N*,*N*-dimethylformamide solution. Cryst Growth Des, 2018, 18: 3132–3137
122 Zhou H, Nie Z, Yin J, *et al.* Antisolvent diffusion-induced growth, equilibrium behaviours in aqueous solution and optical properties of $CH_3NH_3PbI_3$ single crystals for photovoltaic applications. RSC Adv, 2015, 5: 85344–85349
123 Grancini G, D'Innocenzo V, Dohner ER, *et al.* $CH_3NH_3PbI_3$ perovskite single crystals: surface photophysics and their interaction with the environment. Chem Sci, 2015, 6: 7305–7310
124 Wehrenfennig C, Liu M, Snaith HJ, *et al.* Charge-carrier dynamics in vapour-deposited films of the organolead halide per-

ovskite $CH_3NH_3PbI_{3-x}Cl_x$. Energy Environ Sci, 2014, 7: 2269–2275
125 Tidhar Y, Edri E, Weissman H, *et al.* Crystallization of methyl ammonium lead halide perovskites: implications for photovoltaic applications. J Am Chem Soc, 2014, 136: 13249–13256
126 Saidaminov MI, Adinolfi V, Comin R, *et al.* Planar-integrated single-crystalline perovskite photodetectors. Nat Commun, 2015, 6: 8724
127 Ding J, Du S, Zuo Z, *et al.* High detectivity and rapid response in perovskite $CsPbBr_3$ single-crystal photodetector. J Phys Chem C, 2017, 121: 4917–4923
128 Dursun I, De Bastiani M, Turedi B, *et al.* $CsPb_2Br_5$ single crystals: synthesis and characterization. ChemSusChem, 2017, 10: 3746–3749
129 Peng W, Wang L, Murali B, *et al.* Solution-grown monocrystalline hybrid perovskite films for hole-transporter-free solar cells. Adv Mater, 2016, 28: 3383–3390
130 Yang Z, Xu Q, Wang X, *et al.* Large and ultrastable all-inorganic $CsPbBr_3$ monocrystalline films: low-temperature growth and application for high-performance photodetectors. Adv Mater, 2018, 30: 1802110
131 Yang Z, Lu J, ZhuGe M, *et al.* Controllable growth of aligned monocrystalline $CsPbBr_3$ microwire arrays for piezoelectric-induced dynamic modulation of single-mode lasing. Adv Mater, 2019, 31: 1900647
132 Pascoe AR, Gu Q, Rothmann MU, *et al.* Directing nucleation and growth kinetics in solution-processed hybrid perovskite thin-films. Sci China Mater, 2017, 60: 617–628
133 Zhou Y, Game OS, Pang S, *et al.* Microstructures of organometal trihalide perovskites for solar cells: their evolution from solutions and characterization. J Phys Chem Lett, 2015, 6: 4827–4839
134 LaMer VK, Dinegar RH. Theory, production and mechanism of formation of monodispersed hydrosols. J Am Chem Soc, 1950, 72: 4847–4854
135 Cao G, Wang Y. Nanostructures and Nanomaterials: Synthesis, Properties and Applications. 2nd Edition. London: Imperial College Press, 2004
136 Huang F, Li M, Siffalovic P, *et al.* From scalable solution fabrication of perovskite films towards commercialization of solar cells. Energy Environ Sci, 2019, 12: 518–549
137 Lu J, Chen SC, Zheng Q. Defect passivation of $CsPbIBr_2$ perovskites for high-performance solar cells with large open-circuit voltage of 1.28 V. ACS Appl Energy Mater, 2018, 1: 5872–5878
138 Liang J, Zhao P, Wang C, *et al.* $CsPb_{0.9}Sn_{0.1}IBr_2$ based all-inorganic perovskite solar cells with exceptional efficiency and stability. J Am Chem Soc, 2017, 139: 14009–14012
139 Gao LL, Liang LS, Song XX, *et al.* Preparation of flexible perovskite solar cells by a gas pump drying method on a plastic substrate. J Mater Chem A, 2016, 4: 3704–3710
140 Li X, Bi D, Yi C, *et al.* A vacuum flash-assisted solution process for high-efficiency large-area perovskite solar cells. Science, 2016, 353: 58–62
141 Xu Y, Zhu L, Shi J, *et al.* Efficient hybrid mesoscopic solar cells with morphology-controlled $CH_3NH_3PbI_{3-x}Cl_x$ derived from two-step spin coating method. ACS Appl Mater Interfaces, 2015, 7: 2242–2248
142 Yang WS, Park BW, Jung EH, *et al.* Iodide management in formamidinium-lead-halide-based perovskite layers for efficient solar cells. Science, 2017, 356: 1376–1379
143 Kim YH, Cho H, Heo JH, *et al.* Multicolored organic/inorganic hybrid perovskite light-emitting diodes. Adv Mater, 2015, 27: 1248–1254
144 Tan ZK, Moghaddam RS, Lai ML, *et al.* Bright light-emitting diodes based on organometal halide perovskite. Nat Nanotech, 2014, 9: 687–692
145 Longo G, Pertegás A, Martínez-Sarti L, *et al.* Highly luminescent perovskite-aluminum oxide composites. J Mater Chem C, 2015, 3: 11286–11289
146 Chen B, Bai Y, Yu Z, *et al.* Efficient semitransparent perovskite solar cells for 23.0%-efficiency perovskite/silicon four-terminal tandem cells. Adv Energy Mater, 2016, 6: 1601128
147 Wang N, Cheng L, Si J, *et al.* Morphology control of perovskite light-emitting diodes by using amino acid self-assembled monolayers. Appl Phys Lett, 2016, 108: 141102
148 Zhang X, Wang W, Xu B, *et al.* Thin film perovskite light-emitting diode based on $CsPbBr_3$ powders and interfacial engineering. Nano Energy, 2017, 37: 40–45
149 Zhu W, Zhang Q, Chen D, *et al.* Intermolecular exchange boosts efficiency of air-stable, carbon-based all-inorganic planar $CsPbIBr_2$ perovskite solar cells to over 9%. Adv Energy Mater, 2018, 8: 1802080
150 Rao H, Ye S, Gu F, *et al.* Morphology controlling of all-inorganic perovskite at low temperature for efficient rigid and flexible solar cells. Adv Energy Mater, 2018, 8: 1800758
151 Jeon NJ, Noh JH, Kim YC, *et al.* Solvent engineering for high-performance inorganic-organic hybrid perovskite solar cells. Nat Mater, 2014, 13: 897–903
152 Lou YH, Li M, Wang ZK. Seed-mediated superior organometal halide films by GeO_2 nano-particles for high performance perovskite solar cells. Appl Phys Lett, 2016, 108: 053301
153 Xiao Z, Bi C, Shao Y, *et al.* Efficient, high yield perovskite photovoltaic devices grown by interdiffusion of solution-processed precursor stacking layers. Energy Environ Sci, 2014, 7: 2619–2623
154 Hwang K, Jung YS, Heo YJ, *et al.* Toward large scale roll-to-roll production of fully printed perovskite solar cells. Adv Mater, 2015, 27: 1241–1247
155 Mitzi DB, Prikas MT, Chondroudis K. Thin film deposition of organic-inorganic hybrid materials using a single source thermal ablation technique. Chem Mater, 1999, 11: 542–544
156 Huo C, Liu X, Song X, *et al.* Field-effect transistors based on van-der-Waals-grown and dry-transferred all-inorganic perovskite ultrathin platelets. J Phys Chem Lett, 2017, 8: 4785–4792
157 Du W, Zhang S, Wu Z, *et al.* Unveiling lasing mechanism in $CsPbBr_3$ microsphere cavities. Nanoscale, 2019, 11: 3145–3153
158 Wang Y, Sun X, Chen Z, *et al.* High-temperature ionic epitaxy of halide perovskite thin film and the hidden carrier dynamics. Adv Mater, 2017, 29: 1702643
159 Leyden MR, Meng L, Jiang Y, *et al.* Methylammonium lead bromide perovskite light-emitting diodes by chemical vapor deposition. J Phys Chem Lett, 2017, 8: 3193–3198
160 Sanders S, Stümmler D, Pfeiffer P, *et al.* Chemical vapor deposition of organic-inorganic bismuth-based perovskite films for solar cell application. Sci Rep, 2019, 9: 9774
161 Li G, Che T, Ji X, *et al.* Record-low-threshold lasers based on atomically smooth triangular nanoplatelet perovskite. Adv Funct Mater, 2019, 29: 1805553
162 Wu Z, Chen J, Mi Y, *et al.* All-inorganic $CsPbBr_3$ nanowire based plasmonic lasers. Adv Opt Mater, 2018, 6: 1800674
163 Liu X, Niu L, Wu C, *et al.* Periodic organic-inorganic halide perovskite microplatelet arrays on silicon substrates for room-

temperature lasing. Adv Sci, 2016, 3: 1600137
164 Xing J, Liu XF, Zhang Q, *et al.* Vapor phase synthesis of organometal halide perovskite nanowires for tunable room-temperature nanolasers. Nano Lett, 2015, 15: 4571–4577

Acknowledgements This work was supported by the Ministry of Science and Technology (2016YFA0200700 and 2017YFA0205004), the National Natural Science Foundation of China (21673054, 11874130, 61307120, 61704038 and 11474187) and the Open Research Fund Program of the State Key Laboratory of Low-Dimensional Quantum Physics (KF201902).

Author contributions Wang S mainly drafted the manuscript, while Yang F, Cao Q, Zhong Y, Wang A, and Du W assisted Wang S to complete the literature research, draw up the tables, and discuss the ideas of the article. Liu X led the project.

Conflict of interest The authors declare that they have no conflict of interests.

Shaoli Wang received her MSc degree from Beijing University of Technology in 2011, and PhD degree from the Institute of Chemistry, Chinese Academy of Sciences in 2014. Then she joined the Experiment Center of Forestry in North China, Chinese Academy of Forestry and engaged in material-related scientific research. At the end of August 2019, she joined the research group of Xinfeng Liu at the National Center for Nanoscience and Technology (NCNST) to study the new nano materials.

Xinfeng Liu is a professor at the NCNST, China. He received his PhD in 2011 at NCNST. Then he joined the School of Physical and Mathematical Sciences of Nanyang Technological University, Singapore, as a postdoctoral fellow. He joined the "100-Talents" Program of the Chinese Academy of Sciences in 2015 and became a professor of NCNST since then. His research group mainly focuses on light-matter interaction and ultrafast spectroscopy at micro-to-nanometer scale.

金属卤化物钙钛矿材料生长方法研究进展

王少丽[1,2], 杨凡[2,3], 朱江瑞[2], 操沁璇[2,4], 钟阳光[2], 王傲成[2,3], 杜文娜[2], 刘新风[2,5*]

摘要 钙钛矿材料尤其是金属卤化物钙钛矿具有优异的性能, 如较大的光系数、较高的载流子迁移率、较长的载流子寿命、可调谐的电阻率、较大的X射线衰减系数和简单的处理工艺等. 这些优点使得钙钛矿材料在光电领域, 如太阳能电池、发光二极管、光电探测器、X/γ射线探测器和激光等研究领域引起了广泛关注. 钙钛矿材料的广泛应用依赖于高质量的钙钛矿晶体或薄膜. 截至目前, 已经涌现出众多的钙钛矿生长技术和方法. 本综述分类总结了近年来用于钙钛矿材料生长的主要方法和手段, 包括溶液降温法、逆温结晶法、反溶剂法、旋涂法和化学气相沉积法等. 通过总结与分析, 发现溶液降温法、逆温结晶法、反溶剂法主要用于生长高质量的钙钛矿单晶, 旋涂法在制备钙钛矿薄膜方面具有较大优势, 而化学气相沉积法则在制备多种形貌的微纳钙钛矿材料方面占据优势. 本综述可为科研人员在钙钛矿材料生长方面提供可参考的依据和具体参数.

